8-30

A. 983

WARD-NA-3045-39

MICROSTRUCTURE AND FATIGUE PROPERTIES OF INCONEL 718

GP

APPLIED TECHNOLOGY

XXXX

[illegible] further Distribution by any Holder of this Document or the Data Therein to Third Parties Representing Foreign Interests, Foreign Governments, Foreign Companies and Foreign Subsidiaries or Foreign Divisions of U. S. Companies Should Be Coordinated with the Director, Division of Reactor Development and Demonstration, U. S. Energy Research and Development Administration

MASTER

Westinghouse Advanced Reactors Division

Prepared for the U. S. Energy Research and Development Administration
Division of Reactor Development and Demonstration Under Contract No.
EY-76-C-02-3045-M

UNITED STATES ENERGY RESEARCH AND DEVELOPMENT ADMINISTRATION
OFFICE OF PUBLIC AFFAIRS • TECHNICAL INFORMATION CENTER

XXXXXXX

NOTICE

Available from USERDA Technical Information Center, P. O. Box 62, Oak Ridge, TN 37830

Price: Paper Copy $4.50 (domestic)

Printed in the United States of America
USERDA Technical Information Center, Oak Ridge, Tennessee

DISCLAIMER

WARD-NA-3045-39

MICROSTRUCTURE AND FATIGUE PROPERTIES OF INCONEL 718

Topical Report

P. C. S. Wu

Approved by:

W. E. Ray
Principal Investigator

P. Murray
Project Manager

Prepared for the U. S. Energy Research and Development Administration
Division of Reactor Development and Demonstration
Under Contract No. E(11-1)-3045, Task 2

Submitted to ERDA/CH January 1977

Westinghouse Electric Corporation
Advanced Reactors Division
P. O. Box 158
Madison, Pennsylvania 15663

TABLE OF CONTENTS

LIST OF TABLES

LIST OF FIGURES

LIST OF FIGURES (Continued)

LIST OF FIGURES (Continued)

LIST OF FIGURES (Continued)

SUMMARY

Low-cycle fatigue behavior of Inconel 718 at 1000°F (538°C) in air was investigated. The effect of pre-test annealing and hold-time in compression on the fatigue strength of this material in the double aged condition was studied. Smooth specimens of Inconel 718 were tested in air under conditions of fully reversed axial strain control with various hold-times (0-60 minutes) in compression. In general, specimens solution annealed at 1725°F (940°C) followed by double aging (AMS-5596C) show strain softening while those solution annealed at 1900°F (1038°C) then double aged to AMS-5597A show strain hardening. In addition, results show that some increase in fatigue life, particularly at lower strain ranges, is observed for specimens vacuum annealed at 538°C for 2000 hours before testing. However, hold-time in compression slightly decreases the fatigue life and the amount of decrease in fatigue life increases with increasing hold-time. Coffin-Manson type equations are derived to describe this dependence of the low-cycle fatigue life of the test material on the plastic strain range.

Microstructural characterization of the as-received and post-tested specimens shows that fine grains (ASTM No. 8-9) and heavy precipitation of carbides and other phases along the grain boundaries occurred after the first double aging procedure (AMS-5596C). In contrast, coarse grains (ASTM No. 3-4) and very little precipitate except carbide along the grain boundaries resulted from the second annealing procedure (AMS-5597A). Fractography of the post-test fatigue specimen is characterized by optical and electron microscope. Transgranular cracks prevail in all specimens including those tested with hold-time in compression. Scanning Electron Microscopy (SEM) micrographs and the Electron Dispersive Analysis of X-rays (EDAX) reveal the microcracking of the (Nb, Ti) C type carbides presumably due to stress concentration. Transmission Electron Microscope (TEM) micrographs show fatigue striations in the brittle as well as ductile failure regions. In addition, the substructure including the precipitation morphology of the major strengthening phase (γ'') in double aged Inconel 718 and its fracture mode under the present test conditions were also characterized by TEM.

1.0 INTRODUCTION

The development of a new generation of advanced nuclear reactors imposes severe demands on materials of construction. Such is the case with the advent of the Liquid Metal Fast Breeder Reactor (LMFBR) where high operating temperatures and high neutron fluxes may cause rapid degradation of material properties. Many of the LMFBR components will operate in sodium environments in the high temperature range of 427°C to 593°C for a design life of 30 years. Inconel 718 with its excellent high temperature strength is an attractive structural material for these components. In the present investigation, the low-cycle fatigue properties of Inconel 718 are investigated at elevated temperature in an air environment. The purpose is to provide information which will supplement the in-sodium test results which are being generated under similar conditions for the same material. These data are necessary to evaluate the alloy as to its intended application. In addition, this information will be used to supplement or verify the methods and criteria currently required by the ASME Code and RDT standards in assessing the structural adequacy of critical LMFBR components at high temperature, fast flux, breeder reactor sodium environments.

The substructure and precipitation in nickel-base superalloys have been investigated extensively in the past[1-3] and its strengthening mechanisms characterized.[4] However, little or no information is available on the effect of substructure on the mechanical behavior of these superalloys. Raymond[5] reported that the notch-bar rupture lifes of Inconel 718 and X-750 are extremely sensitive to the presence of a γ' denuded zone adjacent to the grain boundaries. Existence of such a zone renders the materials very notch-brittle. The effect of substructure on the low-cycle fatigue behavior of Inconel 718 has not been reported, and it is the purpose of the present investigation to reveal partially if not wholely the microstructural picture of processes occurring during the strain cycling of Inconel 718.

2.0 EXPERIMENTAL

2.1 Test Equipment

A closed-loop, hydraulically actuated, servo-controlled MTS system 910.84 is used in the present investigation. The system has a capacity of providing a force of 50,000 lb. (22,729 Kg.) for uniaxial-fatigue testing involving push-pull loading. Tests can be controlled by any one of the modes, "load", "strain", or "stroke". In the present investigation, the fatigue testing was conducted in the "strain" control mode.

The test fixture, shown in Figure 1 was designed specifically for the present investigation. The load train rods are made of high temperature alloy, Inconel 601 while the three guide rods and the top and bottom plates are made of carbon steel. A split test furnace with three 3-inch zones was constructed to provide access ports for control and readout thermocouples. Electronic Control Systems (ECS) model 6821 controllers are used for temperature control and the temperature was controlled within $\pm$ 2°C during testing.

A typical sample arrangement and the attachment of the fatigue fixture to the MTS system is shown in Figure 2. In the case of elevated temperature testing, the clip gauge is attached to the extensometer platform. In Figure 3 the temperature control system, hydraulic system, and the readout system for the fatigue testing are shown. The functional performance of the test fixture, high temperature extensometer, and the recording system was checked out to be satisfactory using a Type 304 SS specimen.

2.2 Test Specimen

The test specimens used in the present investigation were all made from the Aerojet Nuclear Company (ANC) standard heat (Cabot, 2180-2-9247) of Inconel 718. The alloy composition and room temperature tensile properties reported by Brinkman and Korth[6] are shown in Table 1. The zero gauge length specimens, fabricated according to W Drawing No. 234C894 shown in Figure 4, were designed to provide information on the fillet strain for calibration purposes. The

test specimens with a uniform gauge length of 0.5 inches were fabricated according to W Drawing No. 234C878 shown in Figure 5 and subsequently grooves were made on the specimen shoulder according to W Drawing No. 5933D59 for attaching the extensometers. Dimensional tolerance and verification of the fabrication procedures are verified by Quality Assurance. The specimens were tested according to Test Plan No. 4066 and Operating Instruction No. 4067. After testing, the specimens were stored for post-test dimensional measurements and microstructural examinations.

Specimen blanks were taken from the longitudinal orientations with respect to the rolling direction of the material. Specimens were rough-machined, heat-treated, and given the final surface preparation after completion of the solution anneal and aging treatments. Solution annealing and aging were conducted in vacuum. All test specimens were heat treated according to one of the four heat treating procedures given in Table 2.

2.3 Test Measurement and Data Reduction

The following basic information was generated in the course of the fatigue testing:

1. Load and strain as a function of time were recorded on a Hewlett-Packard Model 17501A two channel strip chart recorder.
2. Load-strain (hysteresis) loops at 1, 5, 10, 15 and the 20th cycle and at load saturation were recorded on the MTS X-Y chart recorder Model #431.12.
3. Cycles to load saturation and cycles to failure.
4. Temperature range during test and the total temperature-time history.

3.0 RESULTS

3.1 Heat Treatment

The material heat treated according to procedure 1, 1038°C solution anneal plus duplex age (AMS 5597A), has a grain size of ASTM 3-4 and no banding structure (duplex grain size distribution) was observed. The material heat treated according to procedure 2, 940°C solution anneal plus duplex age (AMS 5596C), has a grain size of ASTM 8-9 and also no banding structure was observed. The subsequent vacuum annealing of these materials at 538°C for 2000 hours showed no significant change in grain size. However, massive carbide precipitation and/or agglomeration occurred. The microstructure of these materials is discussed in a latter section. The 0.2% offset yield strengths and the engineering stress-strain curves obtained at 538°C for materials heat treated by procedure 1 and 2 are shown in Figure 6.

3.2 Fatigue Test

All tests in the present investigation were conducted in a calibrated "axial strain control" mode with the clip gauge attached to the high temperature extensometer which was fastened to the specimen shoulders. A calibration run, with a zero gauge length specimen, was conducted at 4×10^{-3} sec^{-1} strain rate and with a triangular and zero mean strain wave form to provide information on the fillet strain before testing of uniform gauge length specimens. In Figure 7 the typical zero gauge length specimen calibration curve at the test temperature (538°C) is shown for material heat treated by procedure 2. It is noted that at about 8000 lbs. (3635 Kg) or 159 Ksi (1.1×10^{-3} MPa) yielding of the specimen occurred. Since the fillet strains are generally elastic and small, the results given in Figure 7 were used for all specimens tested in the present investigation.

Based on the information given in Figure 7, measurements obtained from all uniform gauge length test specimens were calibrated. Results obtained on specimens duplex aged according to AMS 5596C are tabulated in Tables 3 and 4 while results obtained on specimens duplex aged to AMS 5597A are given in Table 5. The strain range versus cycles to failure for specimens heat treated according to procedures 1 and 3 are plotted in Figure 8 while the results for specimens heat treated according to procedures 2 and 4 are shown in Figure 9.

For each test, the load and strain as a function of time were recorded on a Hewlett-Packward two channel strip chart recorder while the hysteresis loops were recorded on the MTS X-Y chart recorder. Cyclic softening was observed for specimens solution annealed at 940°C and duplex aged (AMS 5596C) as shown in Figure 10. For specimens solution annealed at 1038°C and duplex aged (AMS 5597A) cyclic hardening, shown in Figure 11, was observed. At lower strain range, the specimen cyclic softened and/or hardened during the initial 10% of its life and its stress range stabilized throughout the subsequent cycling as is shown in Figure 12. However, at higher strain ranges the specimen showed cyclic softening until its failure as shown in Figure 13. For specimens tested with hold-time in compression the hysteresis loop stabilized very quickly even at high strain ranges as shown in Figure 14.

The cyclic softening and hardening in terms of stress range versus the number of cycles for Inconel 718 solution annealed at 940°C plus duplex aging as well as solution annealed at 1038°C plus duplex aging are shown in Figures 15 and 16, respectively. The response of plastic strain ranges with respect to the number of cycles under cyclic softening and cyclic hardening conditions are shown in Figures 17 and 18, respectively, for the same material.

Least squares curve fitting was performed to obtain second order best fit quadratic equations for the test results obtained in the present investigation with the total strain range ($\Delta\varepsilon_t$) ranging from 0.96% to 2%. The equation is of the following form:

$$\log \Delta\varepsilon_t = A + B \log N_f + C (\log N_f)^2 \qquad (1)$$

Where A, B, and C are constants for a particular heat treatment. Values of these constants are given in Table 6. In addition, the elastic ($\Delta\varepsilon_e$), and the plastic ($\Delta\varepsilon_p$) stabilized strain ranges, based on hysteresis loops at approximately $N_f/2$, versus cycles to failure for the various heat treatments are found to follow the familiar power law relationships,

$$\Delta\varepsilon_p = DN_f^a \quad (2)$$

and

$$\Delta\varepsilon_e = EN_f^b \quad (3)$$

Where D, a, E, and b are constants for a given heat treatment. Values of these constants are given in Table 7.

The stabilized stress amplitude versus plastic strain amplitude derived from the present tests is shown in Figure 19. At large plastic strains ($\Delta\varepsilon_p/2 > 0.1\%$), there is no significant difference among the specimens due to the different heat treatments discussed in the previous section. However, for ($\Delta\varepsilon_p/2$) < 0.1%, the vacuum aged specimens appear to have higher stabilized stress amplitude. The results in Figure 19 can be represented by the following equation:

$$\left(\frac{\Delta\sigma}{2}, \text{ksi}\right) = 147.9 \left(\frac{\Delta\varepsilon_p}{2}\right)^{7.15 \times 10^{-2}} \quad (4)$$

or

$$\left(\frac{\Delta\sigma}{2}, \text{MPa}\right) = 21.2 \left(\frac{\Delta\varepsilon_p}{2}\right)^{7.15 \times 10^{-2}} \quad (5)$$

3.3 Microstructural Characterization

3.3.1 Optical Microscopy

The microstructure of the alloy solution annealed at 940°C and duplex aged (AMS 5596C) is shown in Figure 20 (a). This treatment gives an average grain size of ASTM 8-9. An average grain size of ASTM 3-4 was obtained from the same alloy solution annealed at 1038°C and duplex aged (AMS 5597A) with its microstructure shown in Figure 20 (b). It is noted that there has been less grain-boundary precipitates resulting from heat treatment 1 with respect to heat treatment 2. In Figure 21 the microstructure of Inconel 718 in the as-heat treated (heat treatment 1) and the vacuum aged (2000 hours at 538°C after heat treatment 1) conditions are compared. It is apparent that certain amount of carbide growth and agglomeration had occurred as a result of the vacuum aging. Similar results were observed in the case of heat treatment 2 and the vacuum aged specimens.

Typical morphology of the fractured surface and the "thumb" shaped fatigue crack is shown in Figure 22 (a) while the presence of numerous fine cracks in a direction perpendicular to the applied load is evident in Figure 22 (b). The morphology of the fatigue cracks generated during the fatigue testing are shown in Figures 23 and 24 for alloys heat treated by the processes 1 and 2 respectively. It is important to note that the cracks are trans-granular and they propagate in a direction perpendicular to the loading direction for all materials. It is also shown in Figure 23 (b) that severe plastic deformation, revealed by the slip lines, occurred around the crack tip. However, no slip lines were revealed in specimens solution annealed at 1038°C and duplex aged (AMS 5597A) as shown in Figure 24 (b). No significant difference was observed on the cracking of the vacuum aged specimens. However, for specimens tested with hold-time in compression, numerous short and blunt cracks were observed, while a few sharp and deep penetrating cracks were observed in specimens tested without hold-time as shown in Figure 25.

3.3.2 Transmission Electron Microscopy

The substructure of the test material, Inconel 718, was characterized in both pre-test and post-test conditions by transmission electron microscopy

(TEM). The typical brittle as well as ductile failure morphology on a fractured fatigue specimen is shown in the TEM replica micrographs in Figure 26. Striations were observed mainly in the brittle failure regions, however, it was also present occasionally in the ductile failure regions.

Carbide precipitation along the grain boundaries, as well as the twin boundaries, is shown in Figure 27 for the test material heat treated according to procedure No. 2 in the pre-test condition. The presence of both gamma prime (γ') phase (Ni_3Al, Ti) and gamma double prime (γ'') phase (Ni_3Nb) in the $[\bar{1}20]$ zone is shown in Figure 28 (a) while the presence of γ'' phase is evident in the superlattice dark-field micrograph shown in Figure 28 (b) for the same material in the pre-test condition. The reflection indexed 1 1/2 0 in Figure 28 (b) could only be produced by the [010] variant of the bct (body center tetragonal) γ'' phase because the allowed reflections for the bct γ'' precipitate are given by $(h+k+l)_{bct} = 2n$, where n is an integer. The substructure of the same material in the post-test condition is shown in Figure 29. It is noted that the slip lines stopped at the carbides which precipitated along the grain boundaries. The superlattice dark-field and bright-field TEM photomicrographs of γ' and γ'' phases are shown in Figure 30 for the same material in post-test conditions.

Similar and large precipitates of γ' and γ'' phases were also observed in the test material heat treated according to procedure 1. In Figures 31 and 32 the presence of γ' and γ'' in the [110] zone is shown for the material in the pre-test condition. TEM superlattice dark-field micrograph of γ' and γ'' for the same material under the same condition is also shown in Figure 33(a) while the superlattice dark-field of γ'' is shown in Figure 33(b). It is obvious that the γ'' precipitates possess disc shaped morphology and are much larger than those shown in Figures 28 and 30 for the same material heat treated by procedure No. 2. The TEM dark-field micrograph of γ' and γ'' phases in the [110] zone is shown in Figure 34 (a) for the same material, heat treated by procedure No. 1, in the post-test condition while the corresponding selective area diffraction pattern is shown in Figure 34 (b). The effect of fatigue testing on the γ'' precipitates is demonstrated in Figure 35. It is important to note that the failure mechanism of the test material is actually

by the cutting of the γ'' precipitates in a direction approximately normal to the reciprocal lattice vector, $\vec{g}$ = 0 1 1/2. In Figure 36 the existence of an ordered body center tetragonal (bct) DO_{22} phase γ'' precipitates in the test material is evident. The streaking of the superlattice reflections in this figure also suggests that the bct γ'' phase has a disc-shaped morphology where the c-axis is normal to the plane of the disc. The reason for streaking was discussed by Paulonis et al.[1]

3.3.3 Scanning Electron Microscopy

Scanning electron microscopy with its large depth of field was employed to characterize the rough fractured surface of the fatigue specimens. The fracture morphology of a specimen heat treated according to procedure No. 2 and fatigue tested at a strain range of 2% is shown in Figure 37. The presence of second phase particles (NbC) and the transgranular fracture is evident in Figure 37 (a) while the microcracks in a direction approximately parallel to the applied load are shown in Figure 37 (b). The appearance of fatigue striations and microcracks is also shown in Figure 38. The chemical composition of the main carbide phase in Inconel 718 was determined by energy dispersive analysis of x-rays (EDAX) to be basically NbC with small amount of Ti as shown in Figure 39.

4.0 DISCUSSION

4.1 Fatigue Test

The main objective of the present investigation is to study the effects of grain size and pre-test annealing on the low-cycle fatigue behavior of Inconel 718. Based on the present results, it appears that the material solution annealed at 1038°C and duplex aged (heat treating procedure 1) has slightly superior low-cycle fatigue life than the same material solution annealed at 940°C and duplex aged (heat treating procedure 2). However, an opposite relationship was reported by Brinkman and Korth[6] in a similar study using the same heat of plate material. The exact reason for this discrepancy is not yet clear but it is very likely caused by substructural variations which will be discussed later.

A comparison of the fatigue results obtained in the present investigation with those reported in the literature[6] for the same heat of alloy shows good agreement for material given the 1038°C solution anneal plus duplex age (ASTM) grain size 3-4) as shown in Figure 40. It is important to note that dual slope occurred at about 4000 cycles for the plastic strain range. The significant decrease in plastic strain range at ∿4000 cycles appears to be consistent for all tests and reflects a change in failure mode. For material heat treated according to procedure 2, significant differences in fatigue life are observed between the current results and the literature values as shown in Figure 41. The larger scattering in fatigue life for the fine-grain material (ASTM 8-9) is consistent with the reported room-temperature fatigue properties of annealed and aged (AMS 5596B) Inconel 718 forging specimens.[7] Their results show that grain size is a major factor in achieving high fatigue strength. However, the effect of grain size on room temperature endurance limit (10^8 cycles) of Inconel 718 plate annealed and aged to AMS 5596B shows that the scattering of the data increases with decreasing grain size as shown in Figure 42.

Hold-time in compression slightly decreases the fatigue life of the test material as shown in Figure 41. The stress in a specimen tested with hold-time is reduced due to relaxation. However, cyclic stress-strain relations

in terms of the minimum compressive stress (σ_{min}) versus total strain range ($\Delta\varepsilon_t$) was found unaffected by the hold-time. A similar feature was observed on the cyclic stress-strain relation with the maximum tensile stress (σ_{max}). This indicates that both the maximum tensile stress (σ_{max}) and the minimum compressive stress (σ_{min}) in a cycle were affected only by the strain range ($\Delta\varepsilon_t$) and independent of the relaxation behavior of the stress during hold-time.

The significant change in surface conditions for the specimens tested with hold-time is the presence of numerous short and blunt cracks in contrast to a few sharp and deep penetrating cracks for specimens tested in a straight push-pull mode. The creep damage during the hold-time in compression is apparently very small, however, surface extrusions produced during the hold-time in compression may provide preferential sites for crack initiation. This may account for the appearance of numerous surface cracks mentioned before. Since crack propagation dictates the low-cycle fatigue life in general and the crack propagates only during the tensile half cycle, it is not surprising that hold-time in compression only slightly decreased the fatigue life of the material tested in the present investigation.

Vacuum annealing at 538°C for 2000 hours has very little effect on the precipitation kinetics of γ' and γ'' phases in Inconel 718, and the consistently higher fatigue life of the vacuum annealed specimens, particularly at lower strain ranges, appears to be related to the additional carbide precipitation resulting from vacuum annealing.

4.2 Substructure Characterization

Unlike most nickel-base superalloys which derive their high-temperature strength through precipitation of γ' phase, Inconel 718 derives its strength on a dispersion of body-center-tetragonal γ'' phase. Consequently, the precipitation kinetics and the morphology of γ'' phase has significant effect on the mechanical behavior of this material. The presence of the γ'' phase determines not only the stress sensitivity of the creep rate, but also the fatigue resistance and cyclic strain behavior of this alloy. In Table 8, the morphology and distribution of γ'' in Inconel 718 heat treated according to procedures 1 and 2 are characterized. It is important to note that the

total volume fraction (33%) of γ'' phase is the same in material heat treated by both procedures. However, for material solution annealed at 1038°C, the average diameter of γ'' phase is about 5 times larger and the average thickness is about 3 times larger than that solution treated at 940°C. In addition, the average particle spacing is about 4 times larger while the density of γ'' is about two orders of magnitude lower in material heat treated by procedure 1. The initial cyclic hardening of the large grain size material (heat treated by procedure 1) is mainly due to its large interparticle spacing of γ'' while the higher strength and the initial cyclic softening of the fine grain material are because of the smaller interparticle spacing and the high density of γ'' precipitates.

In the present material which contains the dispersed γ'' and γ' phases, the resistance to deformation appears to be by the pinning of dislocations until the applied stress overcomes pinning by cutting through the particles. The massive cutting of γ'' particles shown in Figure 35 (b) further substantiate the massive planar slip deformation mode suggested by Oblak et al.[4] for Inconel 718. They also reported that shear takes place by dislocation pairs, i.e., by $\frac{a}{2}$ <110> pairs. They did not observe shear by glide slip and this may be due to the fact that the alloy, Inconel 718, has low-stacking fault energy which makes the cross slip with screw dislocations more difficult.

CONCLUSION

1. Both γ' and γ'' precipitates were observed in the test material heat treated by all four procedures, but the disc-shaped body center tetragonal (bct) γ'' phase is the major precipitate which amounts to about 33% in volume in all cases. However, the average particle size and the interparticle spacing are about 4 to 5 times longer in material heat treated by procedure #1 (1038°C solution anneal plus duplex age) with respect to the material heat treated by procedure #2 (940°C solution anneal plus duplex age). The difference in γ'' morphology has a significant effect on the cyclic strain behavior of the test material, Inconel 718.

2. Low-cycle fatigue results of coarse grained Inconel 718 show good agreement with those reported by Brinkman and Korth, however, the fatigue life of the fine grained material is lower than the reported values. This discrepancy appears to be due to the large scattering of fatigue data commonly observed on the fine grained Inconel 718.

3. Transgranular cracks were observed in all specimens and the crack propagated in a direction perpendicular to the applied load. For specimens tested without hold-time, a few deep penetrating cracks were observed while for specimens tested with hold-time in compression, numerous short and blunt cracks were observed. This is mainly due to the creep damage (grain boundary sliding) during the hold-time which served to initiate the cracks at the specimen surface.

4. Results obtained in the present investigation substantiate the massive planar slip deformation mode in the alloy Inconel 718. In addition, intense slip bands and some intersecting slip were observed, while internal cracking which apparently associated with the fractured particles such as the NbC was also infrequently observed.

5. Vacuum aging at the test-temperature (538°C) for 2000 hours prior to testing slightly enhanced the low-cycle fatigue resistance

of the material particularly at lower strain ranges. The enhancement may be due to the massive carbide precipitation observed in the vacuum aged samples.

6. Hold-time in compression did not cause any noticeable amount of creep damage as observed metallographically, and it also did not enhance the crack propagation which dictates the low-cycle fatigue life for most materials. Therefore it is not surprising that although numerous surface cracks were observed, hold-time in compression only slightly decreased the low-cycle fatigue life in the present investigation.

7. The cyclic softening of the fine-grained material (940°C solution anneal + duplex age) is mainly due to the break-up of the fine and dense γ'' and γ' phases. However, partial relaxation of microresidual stress set up by the precipitation process may also contribute to the observed cyclic softening phenomenon.

8. The initial cyclic hardening of the coarse grained material (1038°C solution anneal + duplex age) is probably due to the low density of the coarse γ'' particles which allows the matrix alloy to accommodate the plastic deformation in a way similar to that for single phase alloys. In addition, the large particle size of γ'' phase also requires high stress for dislocations to cut through but the larger interparticle spacing tends to decrease the shearing stress. Consequently, the stabilized tensile stress is about the same for both fine grained and coarse grained materials. The subsequent cyclic softening of the coarse grained material is believed to be due to the fracturing of the γ'' precipitates as shown metallographically.

REFERENCE

1. D. F. Paulonis, J. M. Oblak, and D. S. Durvall, "Precipitation in Nickel-Base Alloy 718," Trans. ASM Vol. 62, 1969, pp. 611-622.

2. V. Ramaswamy, P. R. Swann, and D. R. F. West, "Observations on Intermetallic Compound and Carbide Precipitation in Two Commercial Nickel-Base Superalloys," Journal of Less-Common Metals Vol. 27, 1972, pp. 17-26.

3. H. L. Eiselstein, "Metallurgy of a Columbiun-Hardened Nickel-Chromium-Iron Alloy," Advances in the Technology of Stainless Steels and Related Alloys, Special Technical Publication No. 369. Published by the American Society for Testing and Materials, 1965.

4. J. M. Oblak, D. F. Paulonis, and D. S. Duvall, "Coherency Strengthening in Ni Base Alloys Hardened by DO_{22} γ" Precipitates", Metallurgical Transactions Vol. 5, 1974 page 143.

5. E. L. Raymond, "Effect of Grain Boundary Denudation of Gamma Prime on Notch-Rupture Ductility of Inconel Nickel-Chromium Alloys X-750 and 718," Trans. AIME Vol. 239, Sept. 1967, pp. 1415-1422.

6. C. B. Brinkman and G. E. Korth, "Strain Fatigue and Tensile Behavior of Inconel 718 from Room Temperature to 650°C," Journal of Testing and Evaluation, JTEVA, Vol. 2, No. 4, July 1974, pp. 249-259.

7. "Inconel Alloy 718", Technical Bulletin T-39, Huntingdon Alloy Products Division, The International Nickel Company, Inc., West Virginia 25720, Second Edition, 1973.

ACKNOWLEDGEMENT

The author is deeply grateful to Dr. A. L. Chang for his assistance in interpreting of the TEM micrographs. The author also wishes to express his appreciation to Mr. J. R. Kahrs for providing the test specimens, and to Mr. P. N. Flagella and M. L. Manjoine for their valuable suggestions and comments during the course of this work. Administrative assistance from Drs. K. C. Thomas and S. L. Schrock of Westinghouse Advanced Reactors Division is also acknowledged. The author also wishes to express his appreciation to Mr. A. L. Snow for reviewing the manuscript.

TABLE 1

Chemical Composition and Room Temperature Tensile Properties[a] of Inconel 718

AEROJET HEAT IDENTIFYING NUMBER	PLATE THICKNESS IN.	VENDOR AND HEAT NUMBER	ASTM GRAIN SIZE	YIELD STRENGTH KSI	ULTIMATE TENSILE STRENGTH KSI	ELONGATION %
2	0.75	Cabot, 2180-2-9247	8	53.4	109.3	33

	CHEMICAL COMPOSITION, %														
AEROJET HEAT IDENTIFYING NUMBER	C	Mn	Si	P	S	Cr	Co	Mo	Cb+Ta	Ti	Al	Fe	Cr	Ni	B
2	.08	.13	.27	.006	.006	18.6	.33	3.0	5.03	1.02	.58	18.6	.002	51.2	.002

(a) Mill annealed condition

Table 2

Heat Treatment Procedures and Specifications for Inconel 718

Heat Treatment Number	Specification	Procedures
1	AMS 5597A	Solution anneal at 1038 ± 14°C for 2 hr. air-cool, duplex age at 760 ± 8°C, hold to 10 hr., furnace-cool at the rate of 55°C/hr. to 649°C, hold for 8 hr. for a total duplex aging time of 20 hrs., and air-cool.
2	AMS 5596C	Solution anneal at 940 ± 14°C for 2 hr, air-cool, duplex age at 718 ± 8°C, hold 8 hr., furnace-cool at the rate of 56°C/hr. to 621°C, hold for 8 hr. for a total duplex aging time of 18 hrs., and air-cool.
3		2000 hours vacuum aging at 538°C after heat treatment 1.
4		2000 hours vacuum aging at 538°C after heat treatment 2.

Table 4

Low-Cycle Fatigue Data[a] For Inconel 718[b] Tested At 538°C In Air

SAMPLE NO.	STRAIN RANGE		STRESS RANGE AT $N_f/2$		HOLD TIME IN COMPRESSION HRS.	FATIGUE LIFE N_f
	TOTAL %	PLASTIC %	Ksi	MPa		
3[c]	1.90	0.71	276.0	1901.6	0	627
15	1.90	0.94	272.0	1874.1	0	457
19	1.45	0.42	264.0	1818.9	0	1482
7	1.26	0.18	264.0	1818.9	0	2286
11	0.87	0.03	204.0	1405.6	0	SAMPLE DID NOT FAIL AFTER 45,556 CYCLES
27[d]	1.02	0.06	236.0	1626.0	0	3725
29	2.01	0.78	268.0	1846.5	0.5	419
45	1.27	0.17	290.0	1998.1	1.0 HOUR HOLD TIME IN THE FIRST 290 CYCLES	2590

(a) STRAIN RATE: 4×10^{-3} SEC^{-1}
CONTROL MODE: AXIAL STRAIN
WAVE FORM: TRIANGULAR, ZERO MEAN STRAIN

(b) VACUUM AGED AT 538°C FOR 2000 HOURS BEFORE TESTING. THE ALLOY WAS 940°C S.A. + DOUBLE AGEING (AMS-5596C) BEFORE SAMPLE FABRICATION.

(c) SAMPLE WAS OVERHEATED TO 704°C FOR ABOUT 30 MINUTES DURING HEATING UP PERIOD.

(d) SAMPLE WAS INADVERTENTLY COMPRESSED TO 2% DURING THE 2ND CYCLE.

Table 3

Low-Cycle Fatigue Data[a] For Inconel 718[b] Tested At 538°C In Air

SAMPLE NO.	STRAIN RANGE		STRESS RANGE AT $N_f/2$		HOLD TIME HRS.	FATIGUE LIFE N_f
	TOTAL %	PLASTIC %	Ksi	MPa		
9	0.95	0.22	233.6	1609.5	0	2,050
17	0.97	0.15	231.0	1591.6	0	3,340
25	1.96	0.96	286.0	1970.5	0	377
1	2.04	1.09	308.0	2122.1	0	400
39[d]	5.32	3.74	320.0	2204.8	0	12
31	2.01	0.98	258.0	1777.8	0.5[c]	357
55	2.0	0.90	266.0	1832.7	1.0[c]	333

(a) STRAIN RATE: 4×10^{-3} SEC^{-1}
CONTROL MODE: AXIAL STRAIN
WAVE FORM: TRIANGULAR, ZERO MEAN STRAIN

(b) AS-FABRICATED, 940°C S.A. + DOUBLE AGE (AMS-5596C)

(c) COMPRESSION ONLY

(d) SAMPLE SHOWS SLIGHT BUCKLING

Table 5
Low-Cycle Fatigue Data[a] of Inconel 718[b]

SPECIMEN NO.	STRAIN RANGE, %		STRESS RANGE ($\Delta\sigma$) AT $N_f/2$		HOLD TIME IN COMPRESSION, MIN	FATIGUE LIFE (N_f) CYCLES
	TOTAL, $\Delta\epsilon_t$	PLASTIC, $\Delta\epsilon_p$	Ksi	MPa		
40	0.96	0.045	210.7	1451.7	0	12,456
48[c]	0.97	0.045	208.0	1433.1	0	8,137
2	2.0	0.610	274.0	1887.9	0	760
18	2.0	1.050	272.0	1874.1	0	457
56	2.0	0.660	274.0	1887.9	60	639
20[d]	1.04	0.030	210.0	1451.7	0	10,960
12[d]	1.24	0.053	222.7	1534.4	0	6,135
57[d]	1.62	0.315	250.5	1725.9	0	1,569
42[d]	2.0	0.740	274.4	1890.6	0	610
38[d]	2.1	0.750	278.3	1917.5	0	605

(a) CONTROL MODE = AXIAL STRAIN
WAVE FORM = TRIANGULAR, ZERO MEAN STRAIN
STRAIN RATE = 4×10^{-3} SEC^{-1}

(b) 1038°C SOLUTION ANNEAL PLUS DOUBLE AGEING (AMS 5597A)

(c) SPECIMEN WAS TESTED AT 0.76% STRAIN RANGE FOR 10,545 CYCLES BEFORE THE STRAIN RANGE WAS INCREASED TO 0.97%

(d) SPECIMEN WERE VACUUM ANNEALED AT 538°C FOR 2000 HOUR BEFORE TESTING

TABLE 6 BEST FIT POLYNOMIAL CONSTANTS DEFINING THE $\Delta\varepsilon_t$ VERSUS N_f RELATIONSHIP OF INCONEL 718

(Equation 1)

Heat Treatment	A	B	C
2	-0.57	-5.42×10^{-1}	4.05×10^{-2}
3	-2.49	7.46×10^{-1}	-16.98×10^{-2}
1	-1.46	0.31×10^{-1}	-4.22×10^{-2}
4	-1.11	-1.95×10^{-1}	-0.48×10^{-3}

TABLE 7 ELASTIC AND PLASTIC STRAIN RANGE CONSTANTS

(Equation 2 & 3)

Heat Treatment	D	a	E	b
2	8.95	-1.12	12.51×10^{-2}	-4.56×10^{-2}
3	9.85	-1.12	1.17×10^{-2}	-6.85×10^{-2}
1	4.33	-0.994	2.06×10^{-2}	-8.60×10^{-2}
4	10.88	-1.1295	1.91×10^{-2}	-6.14×10^{-2}

Table 8 Morphology and Distribution of γ'' in Inconel 718

Heat Treatment	Average Diameter Å	Average Thickness Å	Average Particle Spacing, Å	Volume Fraction %	Density [a]
1 [b]	1050	210	1210	33	5.68×10^{14}
2 [c]	225	75	310	33	3.42×10^{16}

(a) Number of γ'' particles per cubic centimeter.

(b) Solution annealed at 1038°C and double aged (AMS 5597A0.

(c) Solution annealed at 940°C and double aged (AMS 5596C).

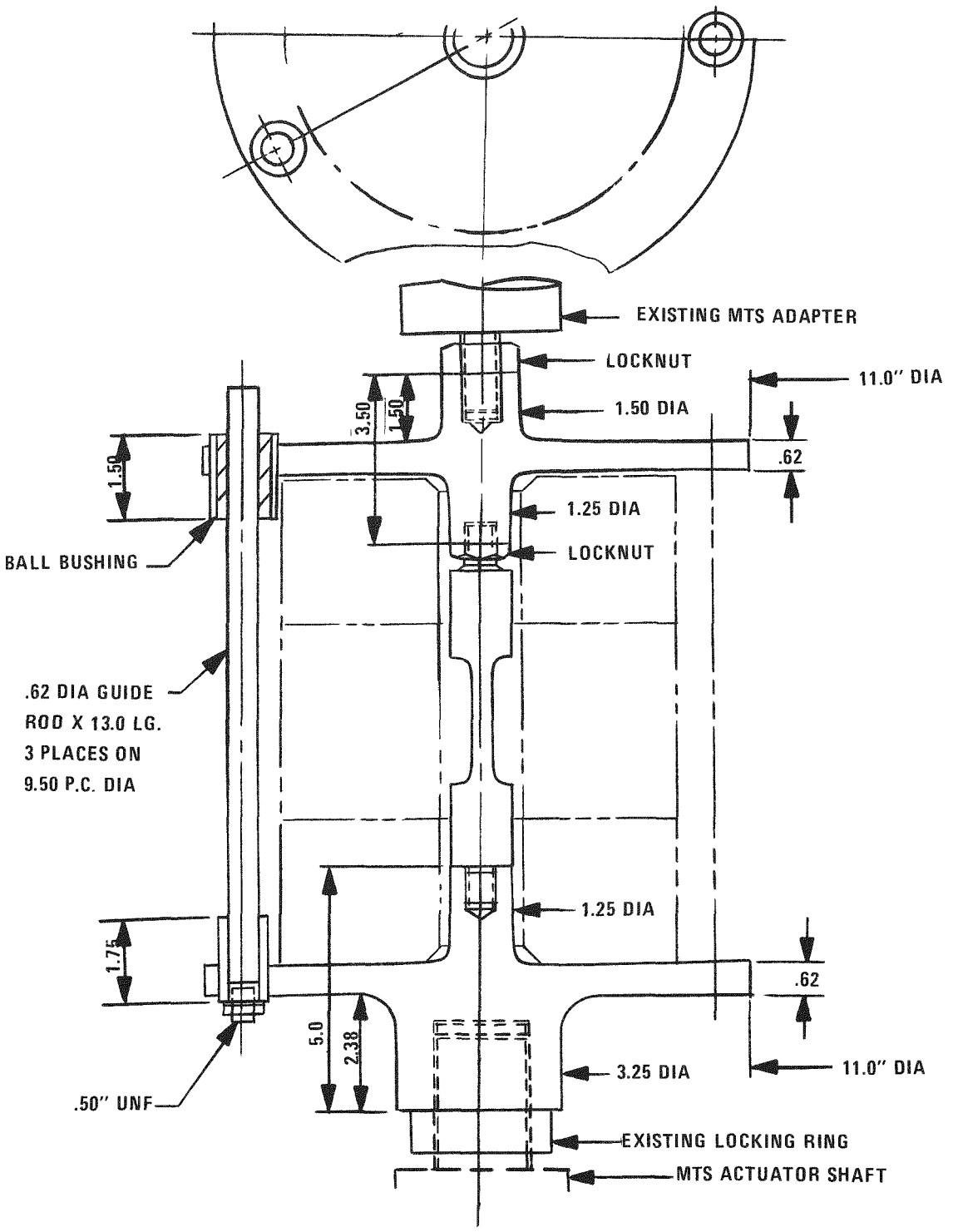

Figure 1. Axial Loading, Low-Cycle Fatigue Test Fixture

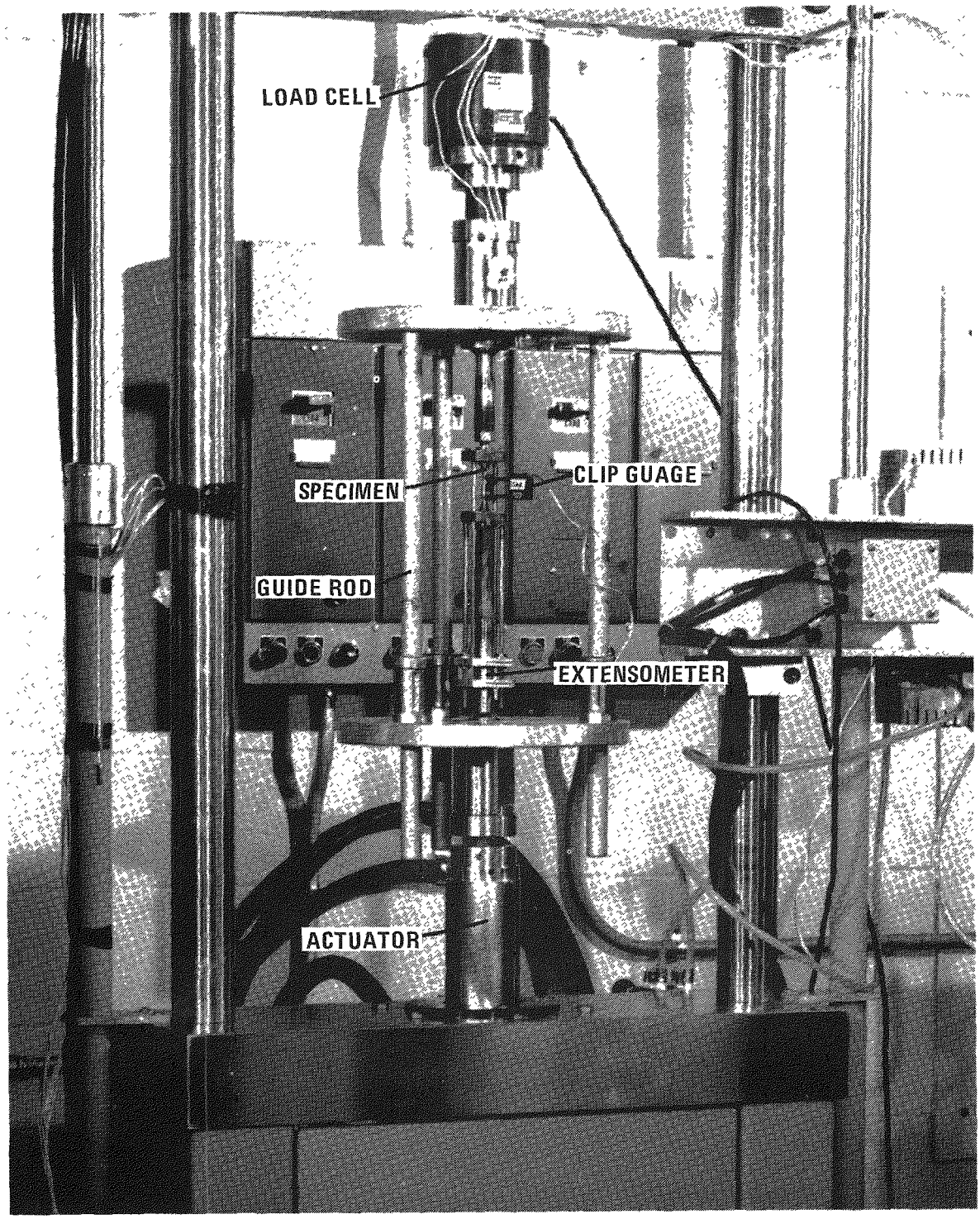

Figure 2 Sample Arrangement and Fatigue Test Fixture

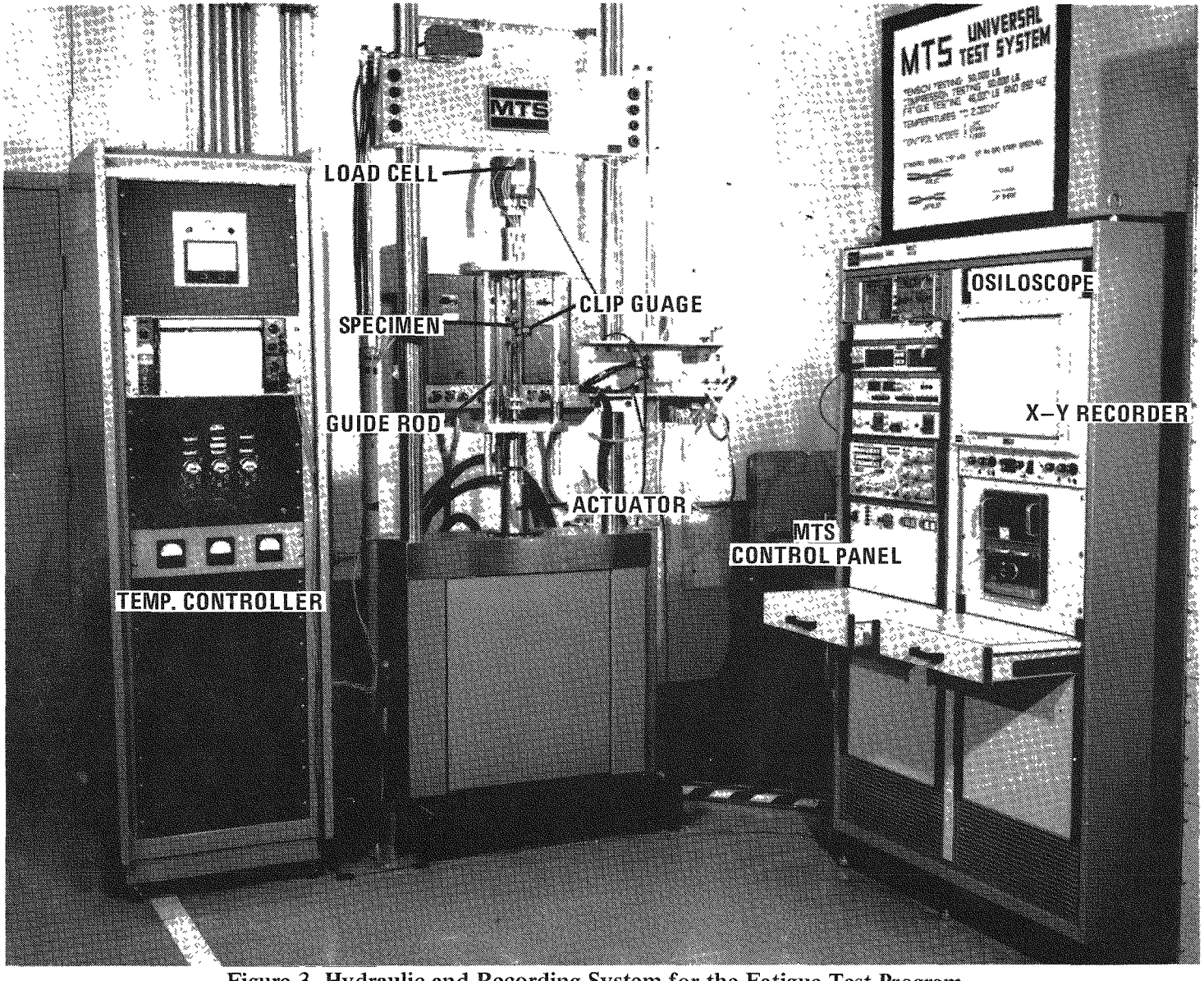

Figure 3 Hydraulic and Recording System for the Fatigue Test Program

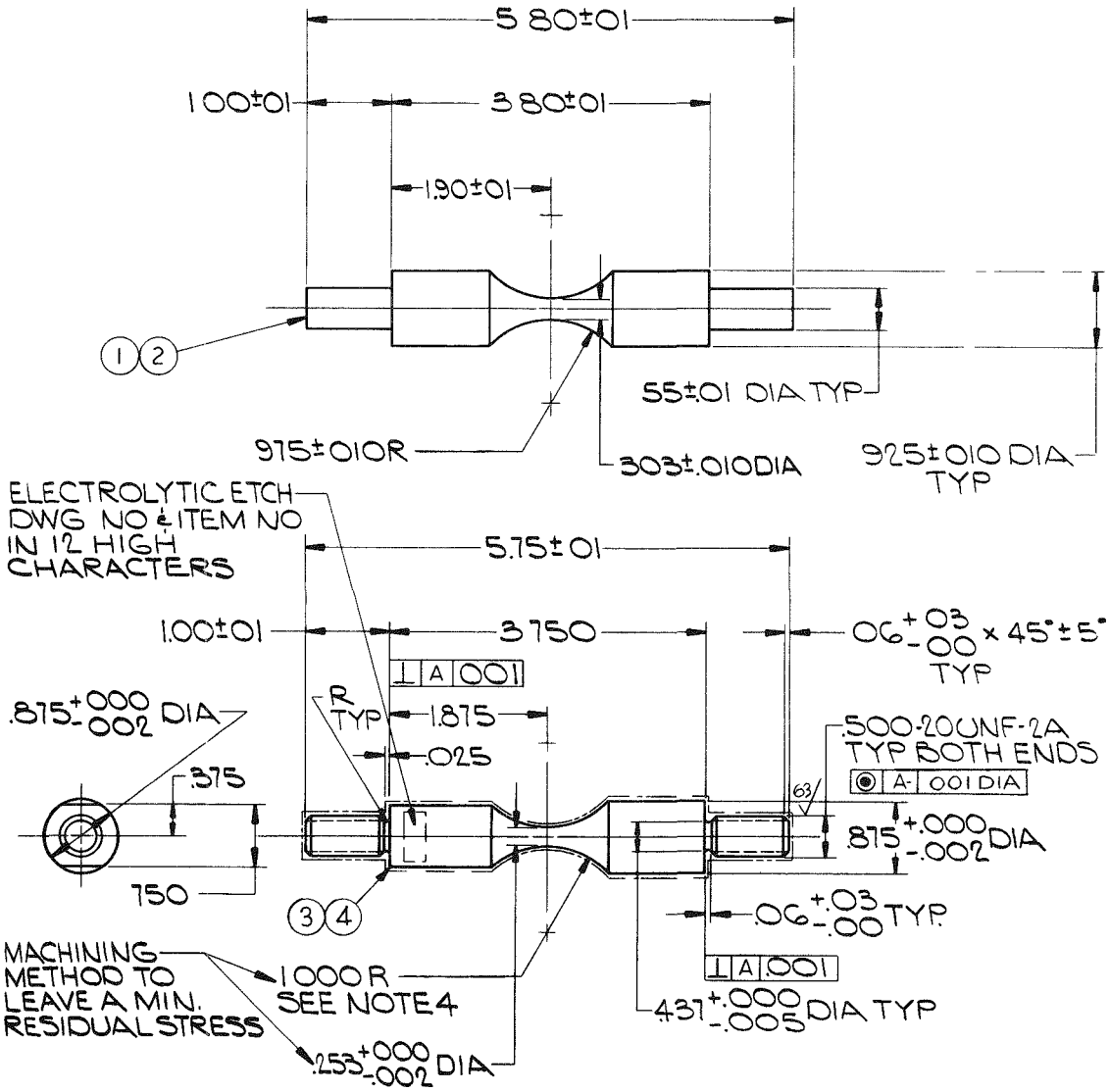

Figure 4. Inconel 718 Zero Gauge Length Fatigue Specimen (AIR)

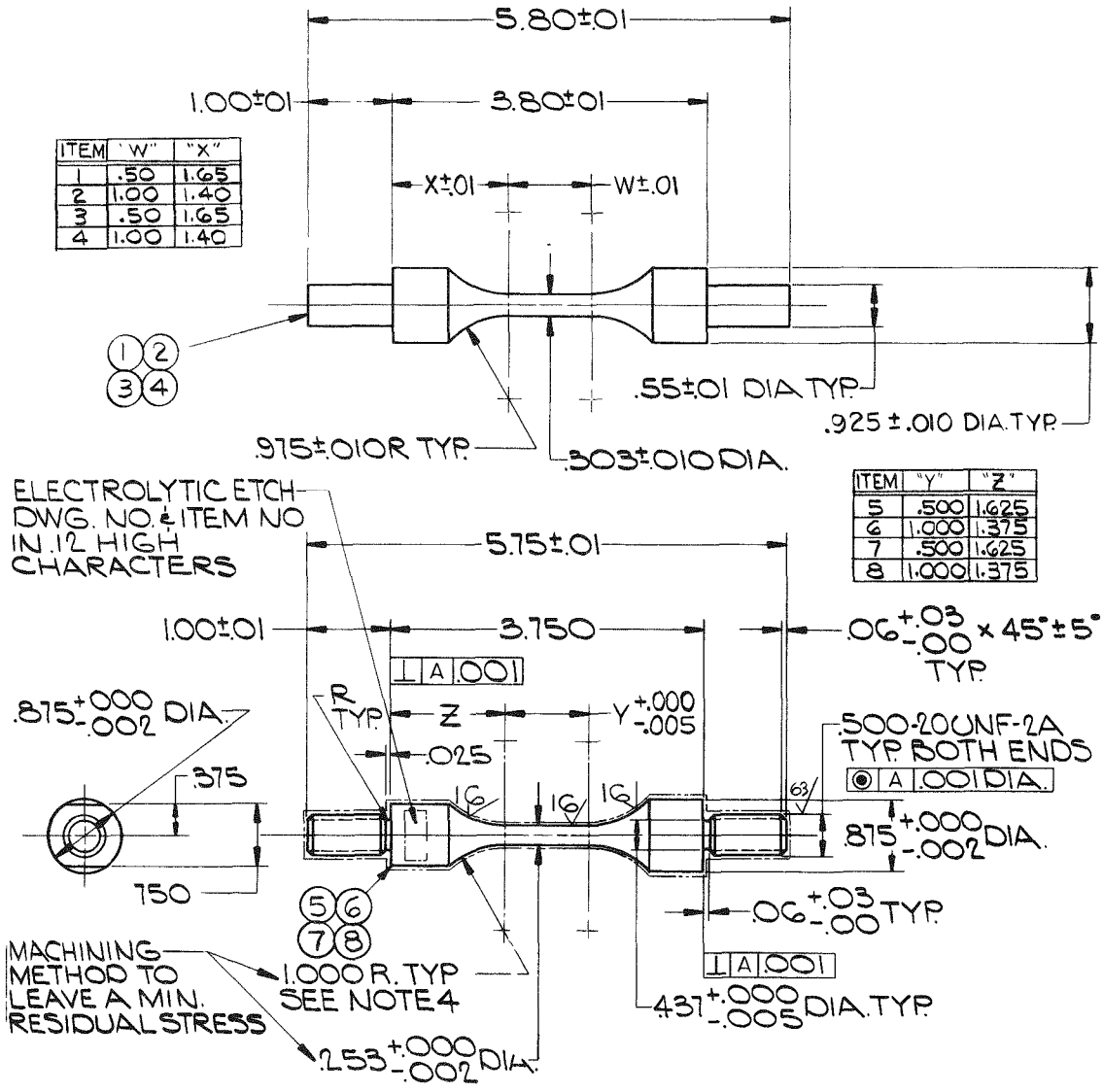

Figure 5. Inconel 718 Fatigue Specimen (AIR)

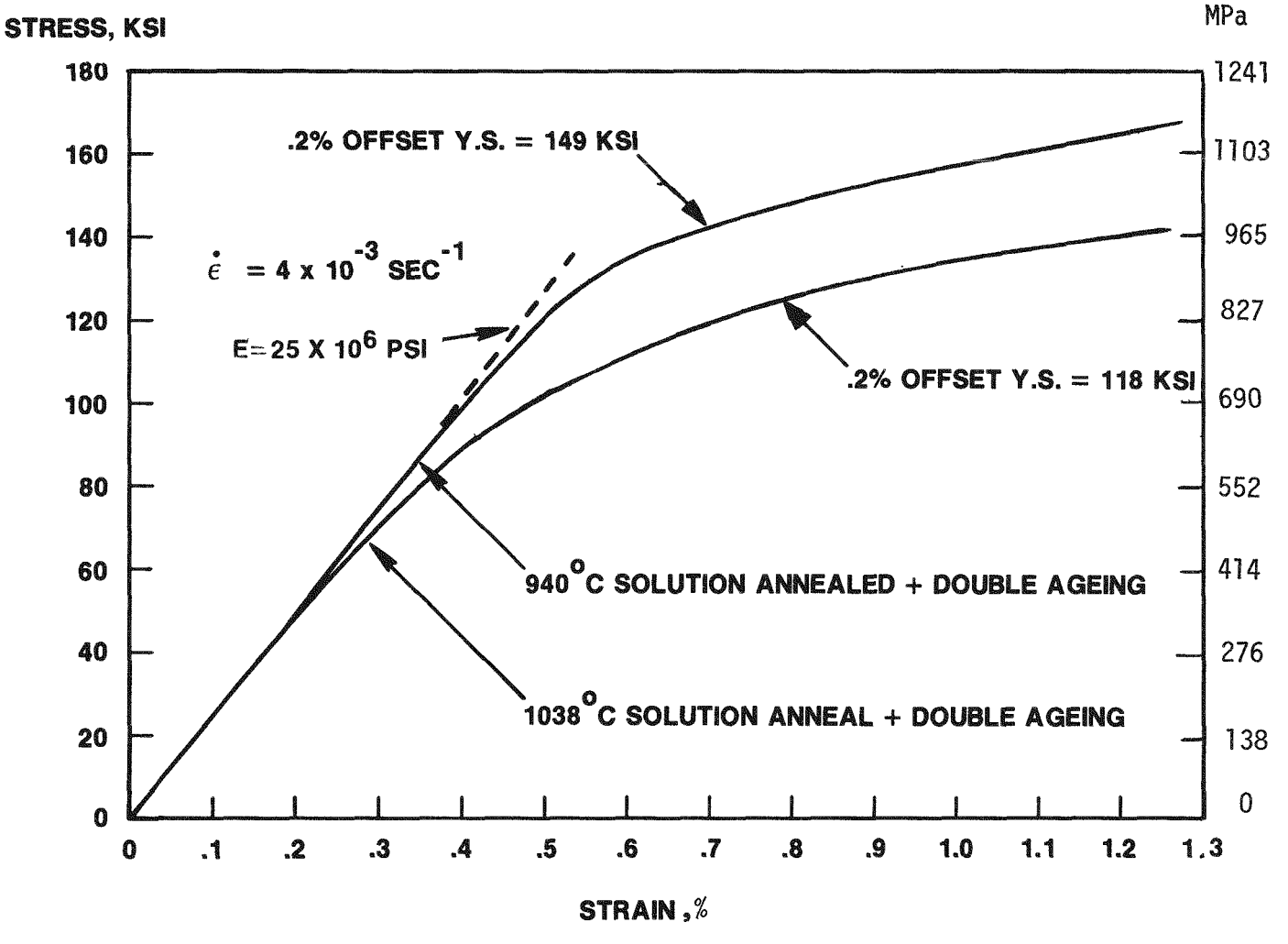

Figure 6 Stress-Strain Curve of INC-718 at 538°C

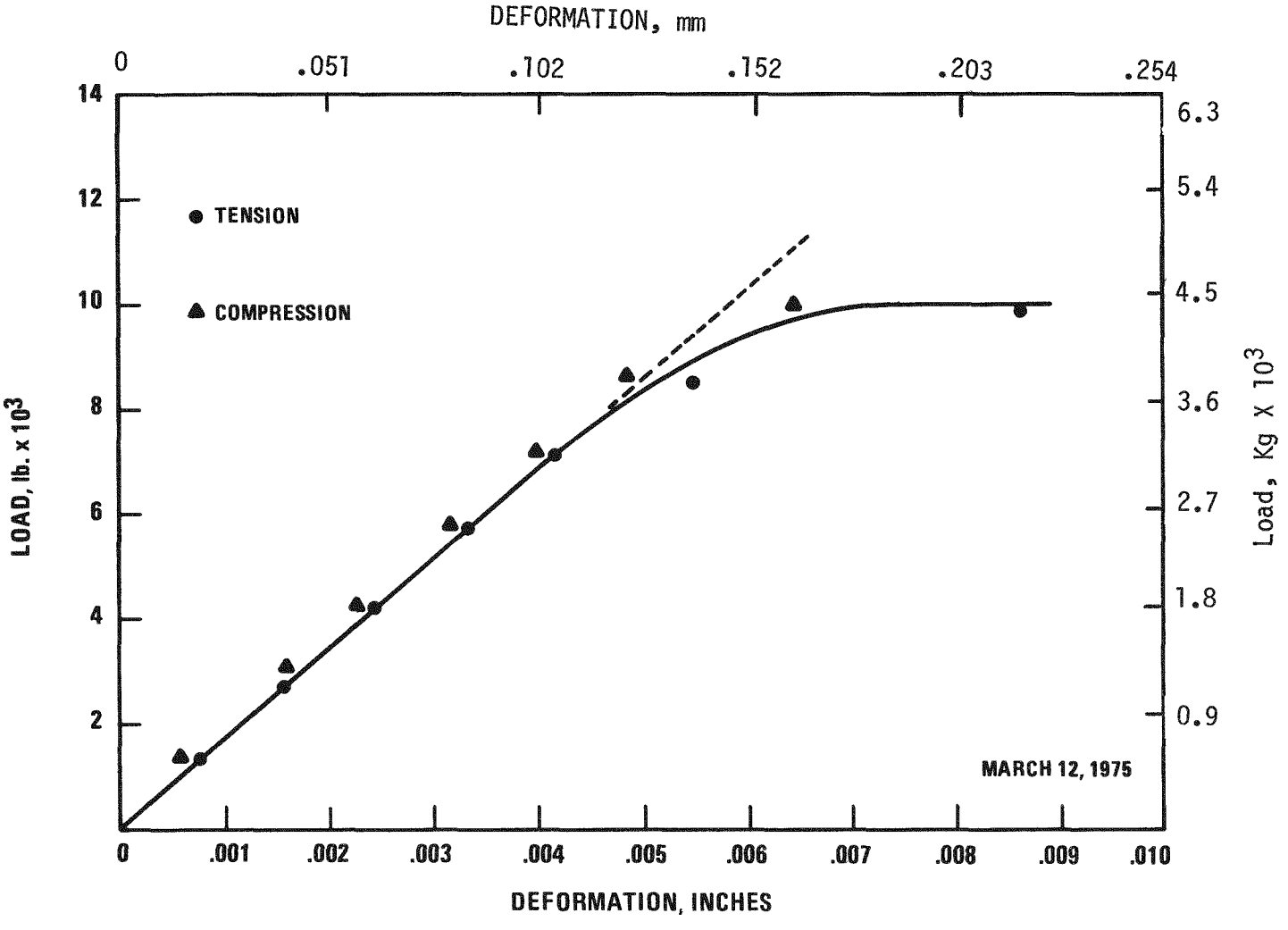

Figure 7. Inconel 718 Zero Gauge Length Fatigue Sample Calibration Curve (Load Control At 538°C In Air)

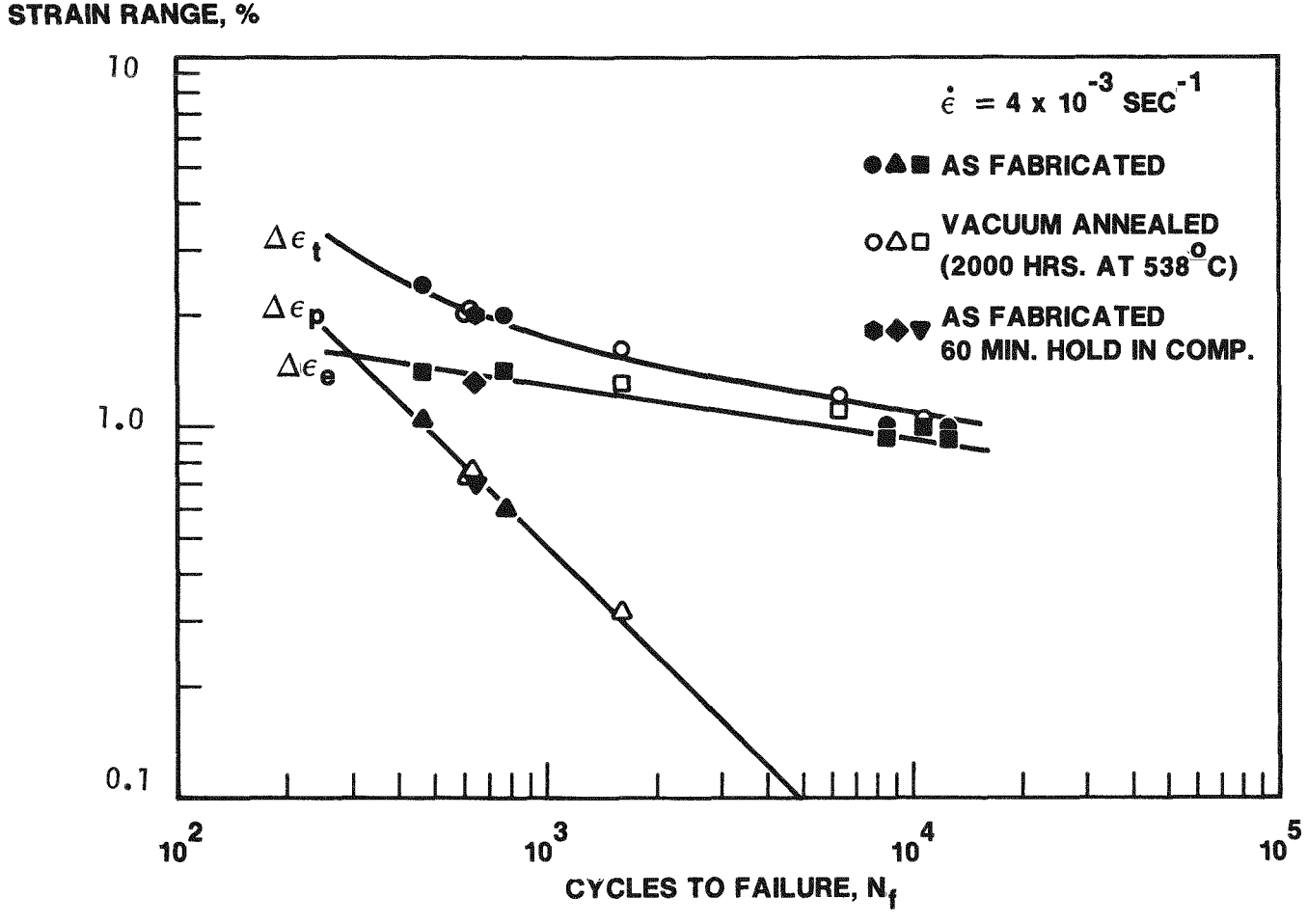

Figure 8. Strain Range Versus Fatigue Life For Inconel 718 (1038°C S.A. + D.A.) At 538°C In Air

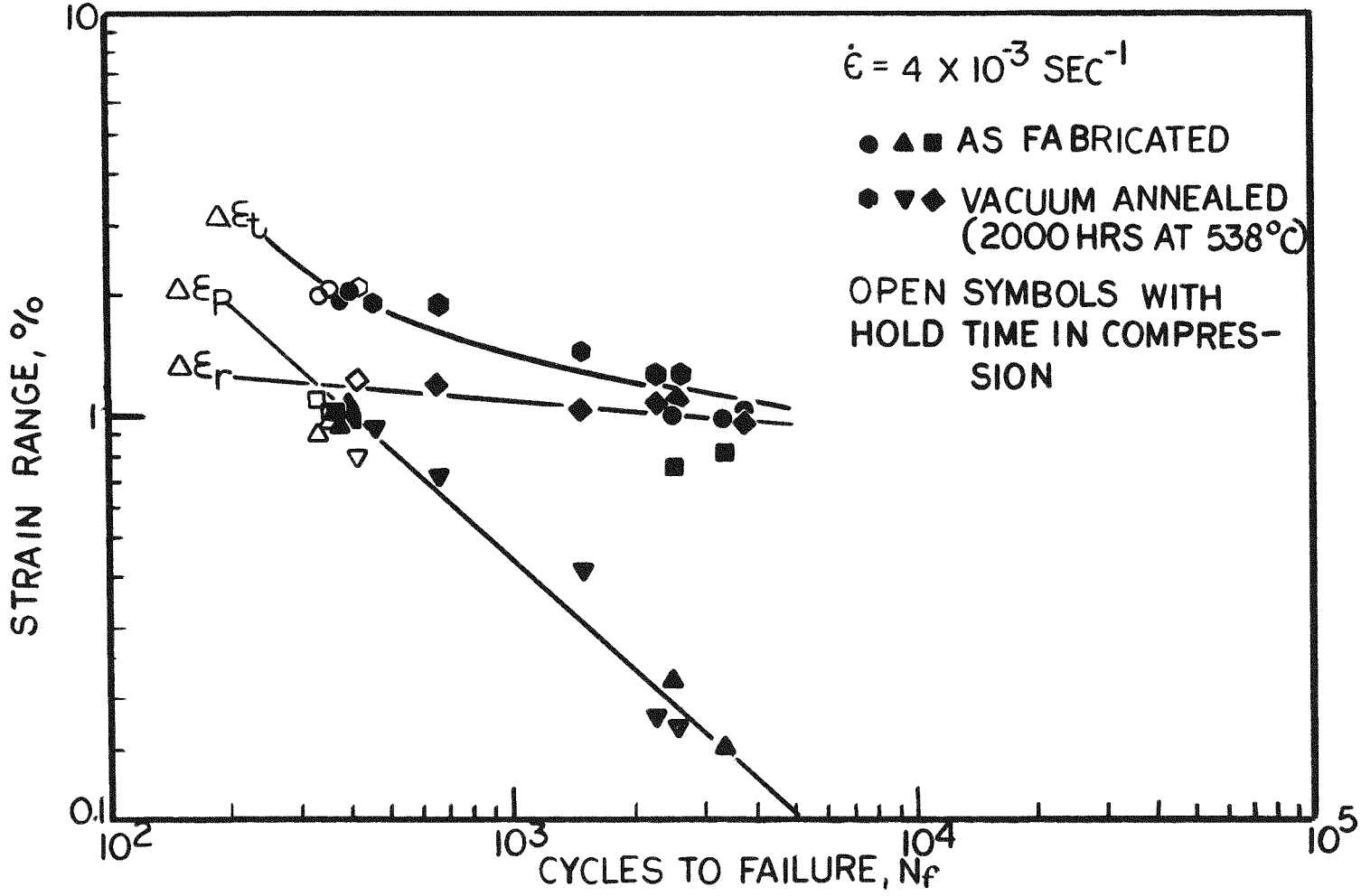

Figure 9. Strain Range Verses Fatigue Life For Inconel 718 (940°C S.A. + D.A.) At 538°C In Air

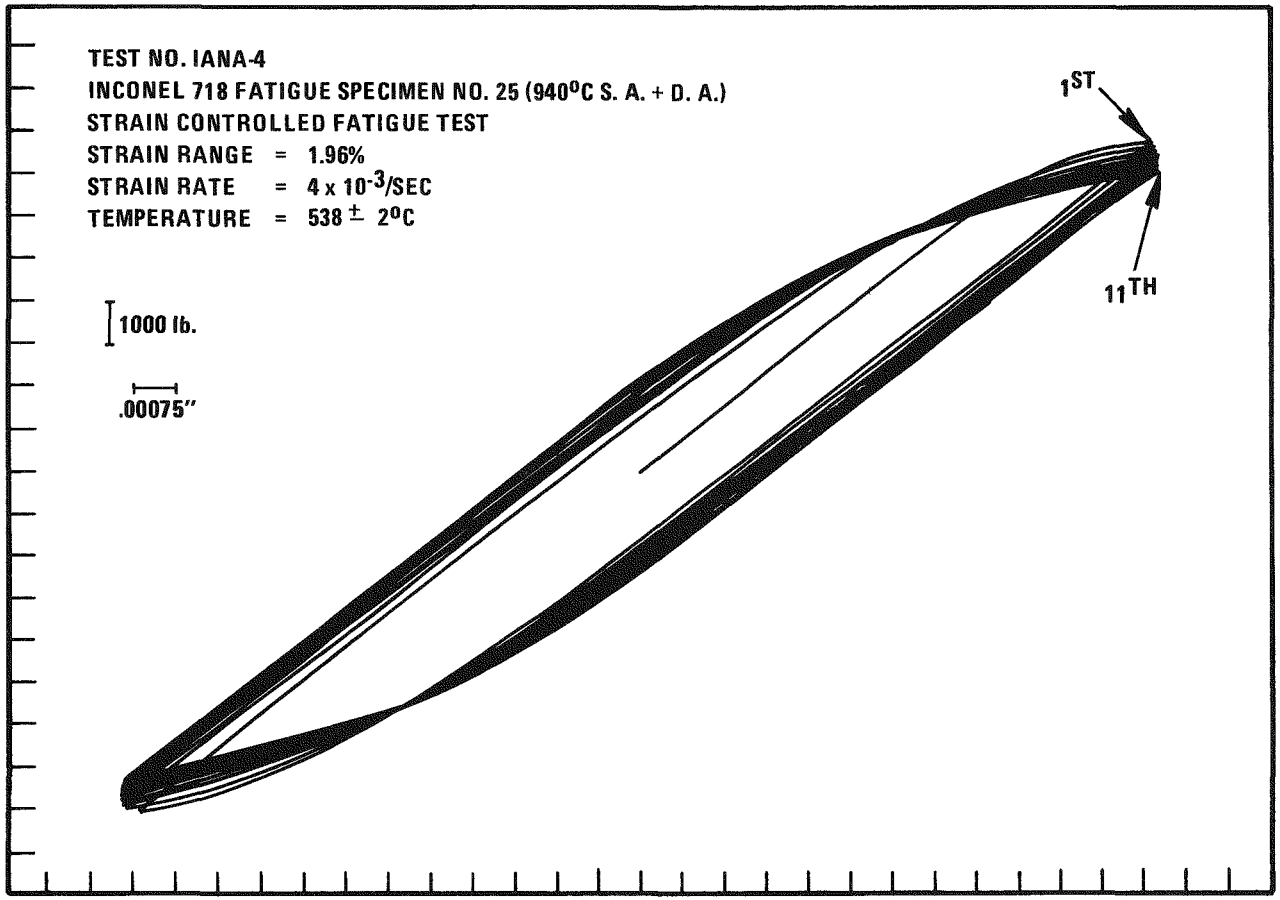

Figure 10. Cyclic Softening Of Inconel 718 At 538° C

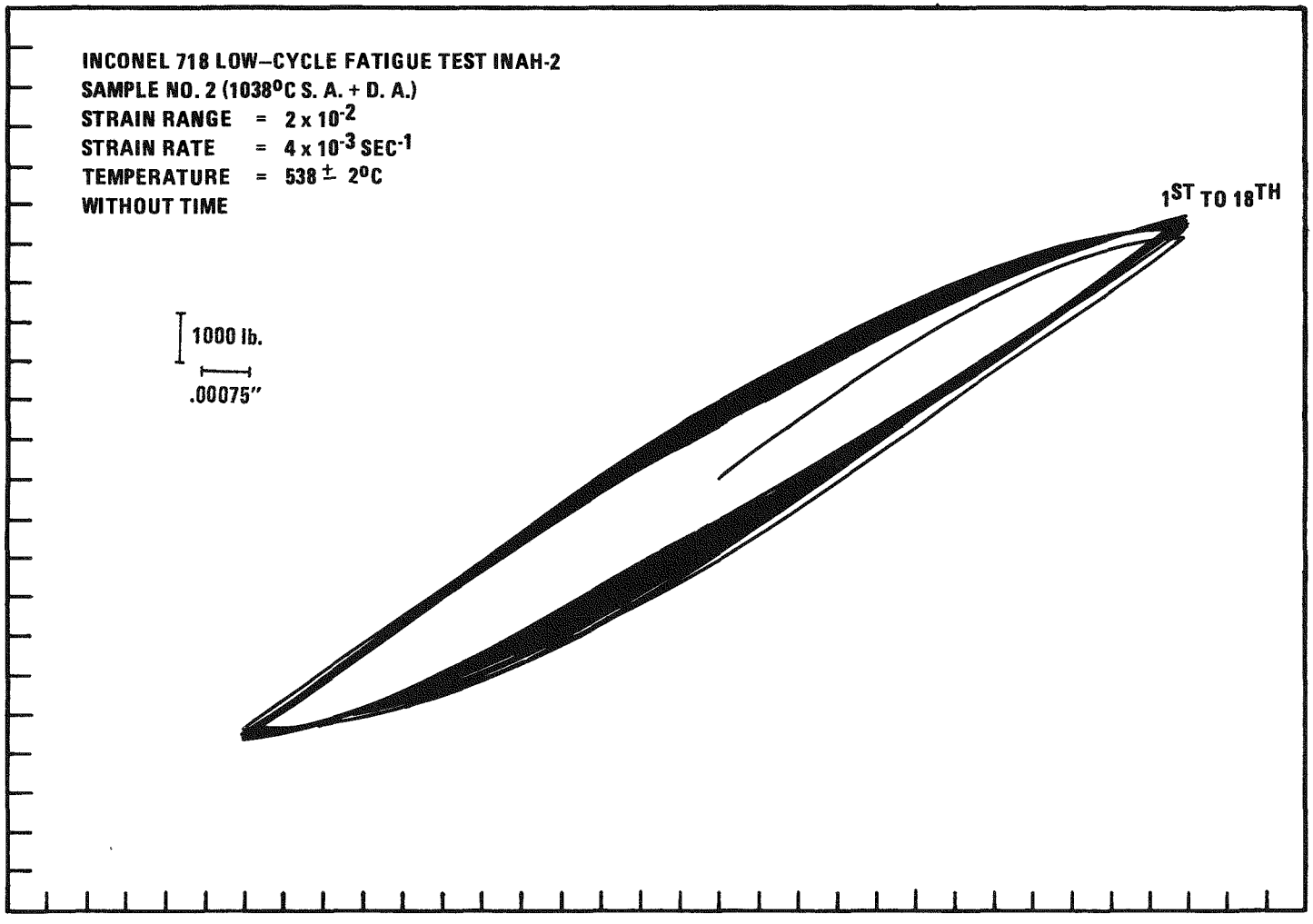

Figure 11. Cyclic Hardening Of Inconel 718 At 538°C

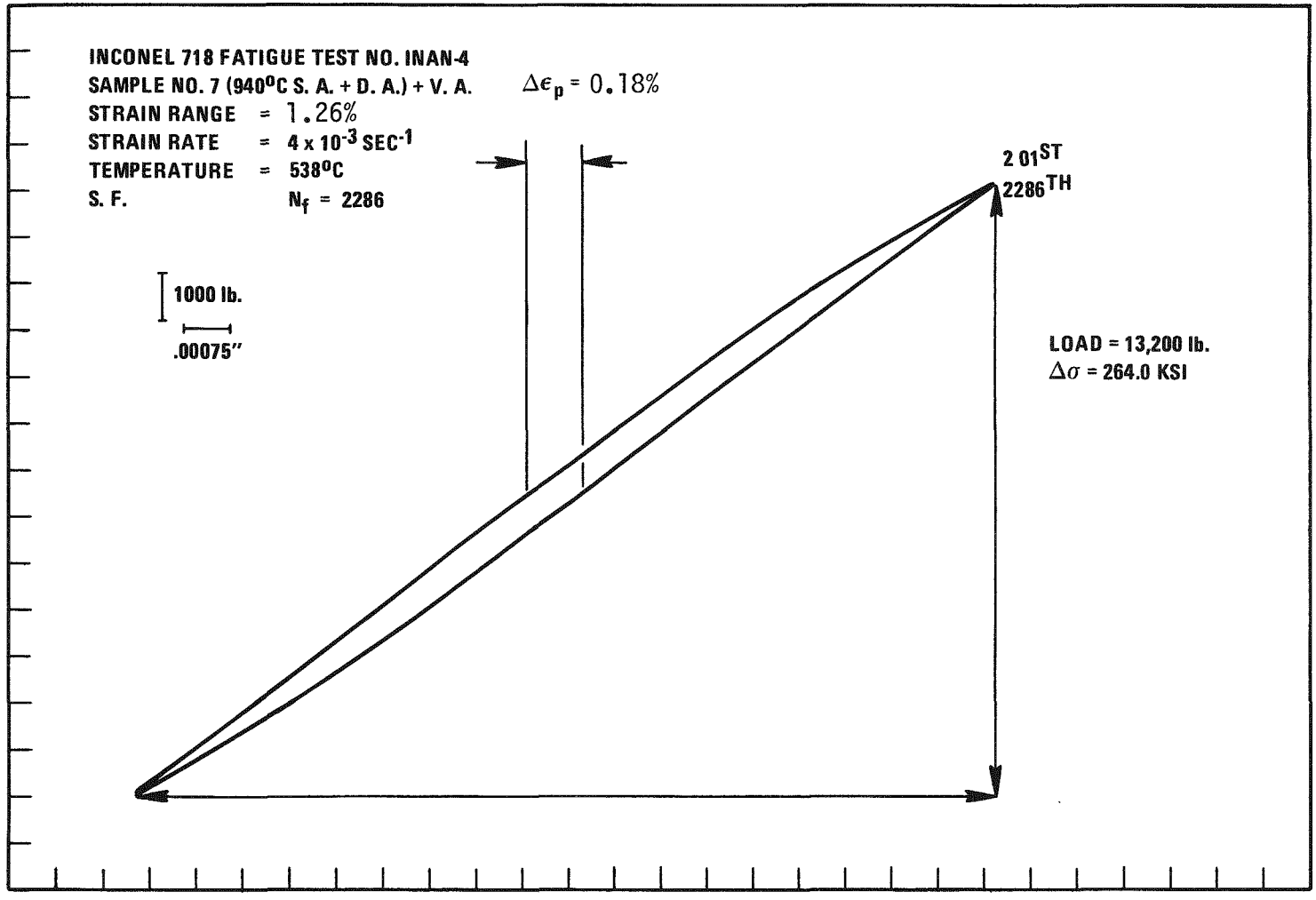

Figure 12. Stabilized Hysterests Loop Of Inconel 718 At 538°C

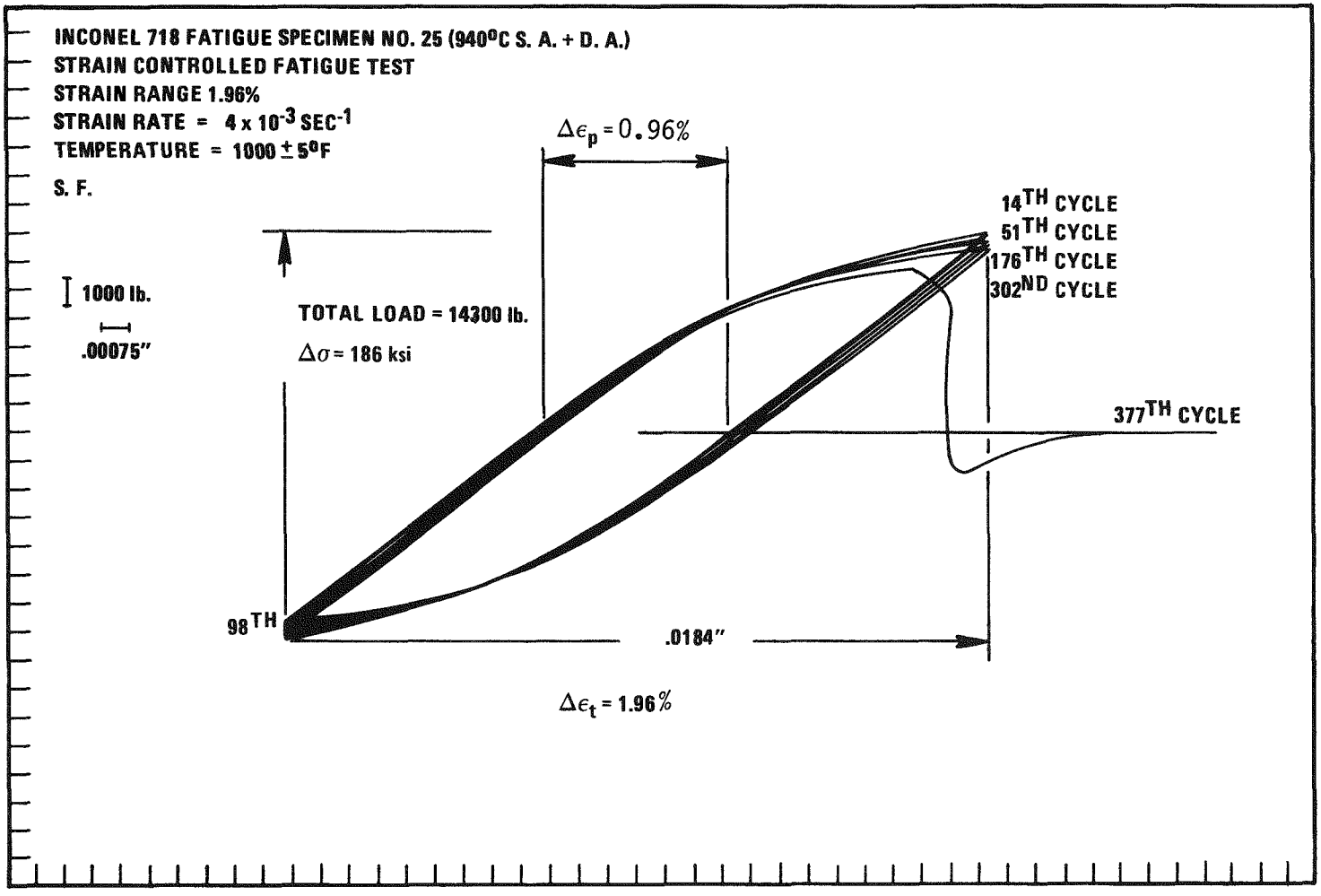

Figure 13. Cyclic Softening Of Inconel 718 At 538°C

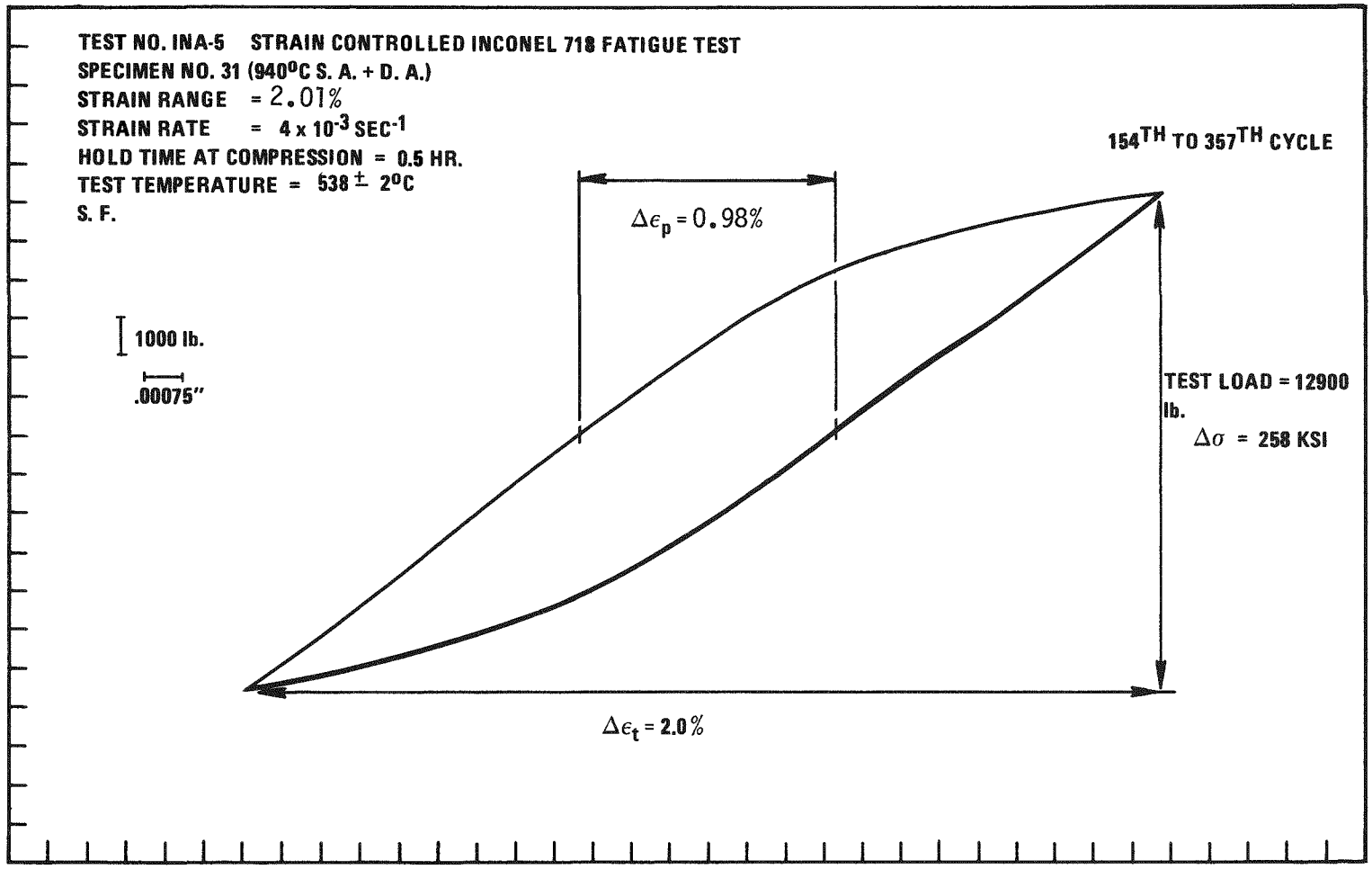

Figure 14. Stabilized Hysterests Loop For Inconel 718 At 538°C

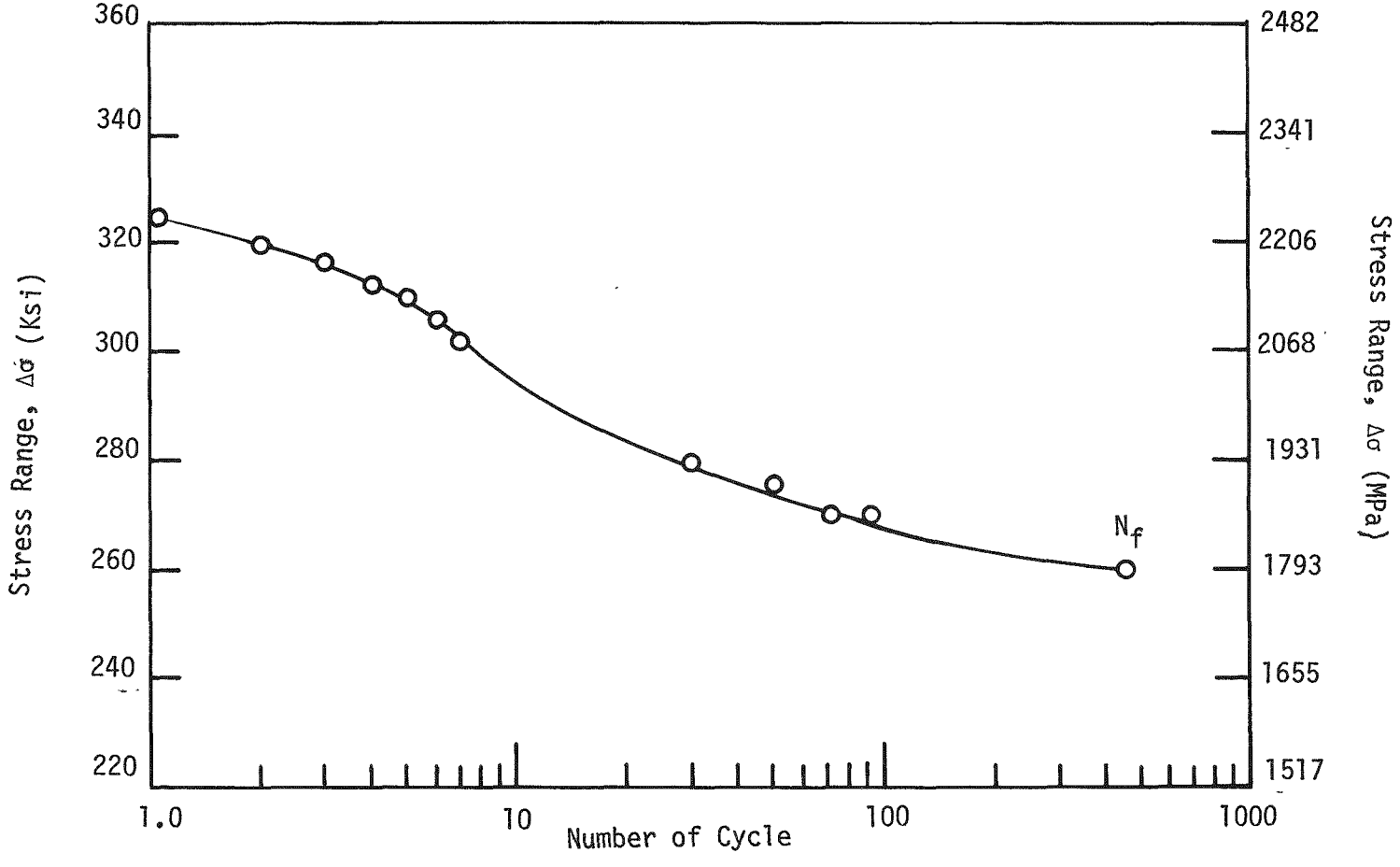

Figure 15. Cyclic Softening of Inconel 718 (940°C S.A. + D. A.) at 538°C in Air With 1.9% Strain Range and 4 X 10^{-3} Sec^{-1} Strain Rate

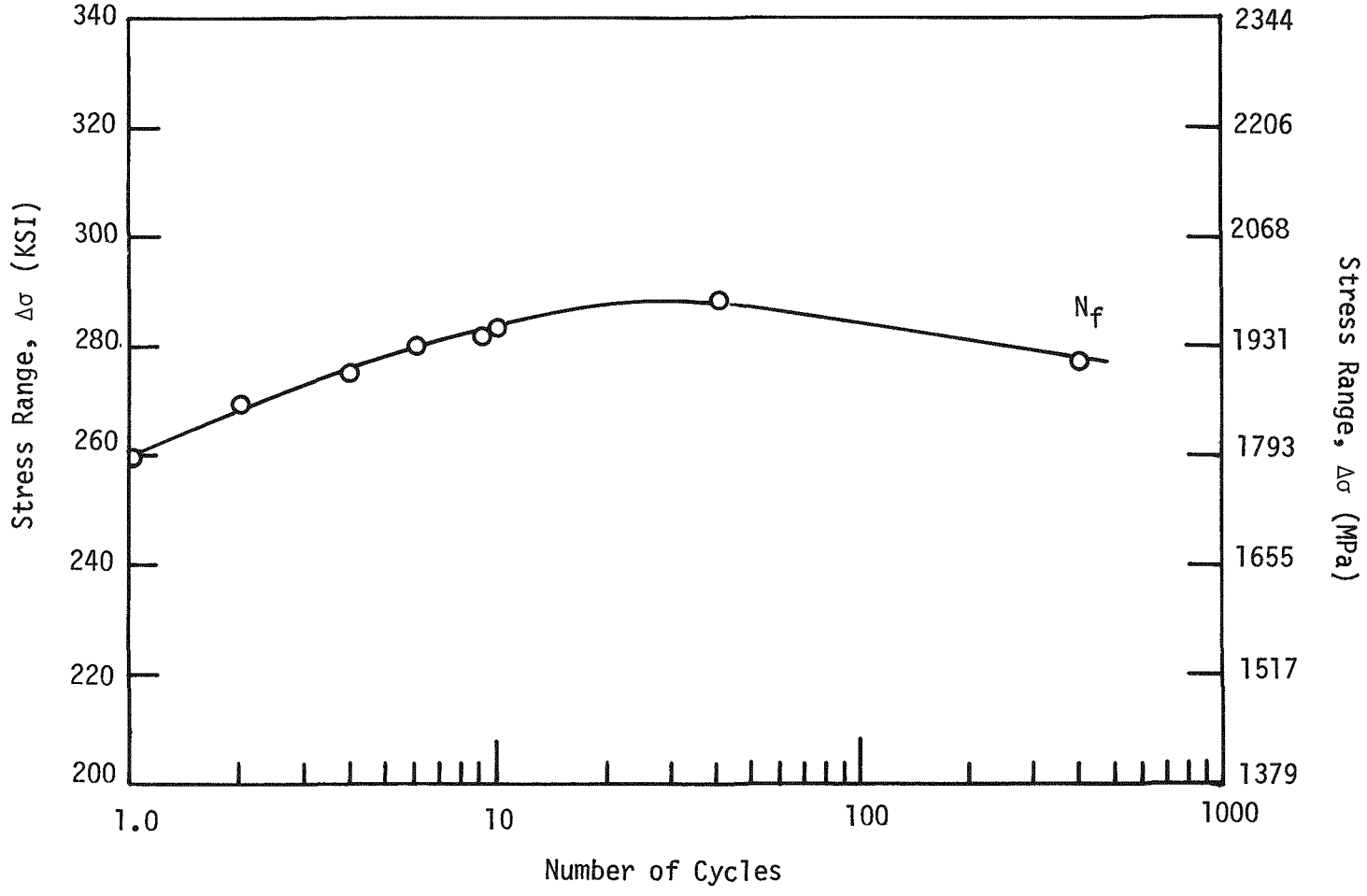

Figure 16. Cyclic Hardening of Inconel 718 (1038°C S.A. + D.A.) at 538°C in Air With 2.0% Strain Range and 4 X 10^{-3} Sec^{-1} Strain Rate

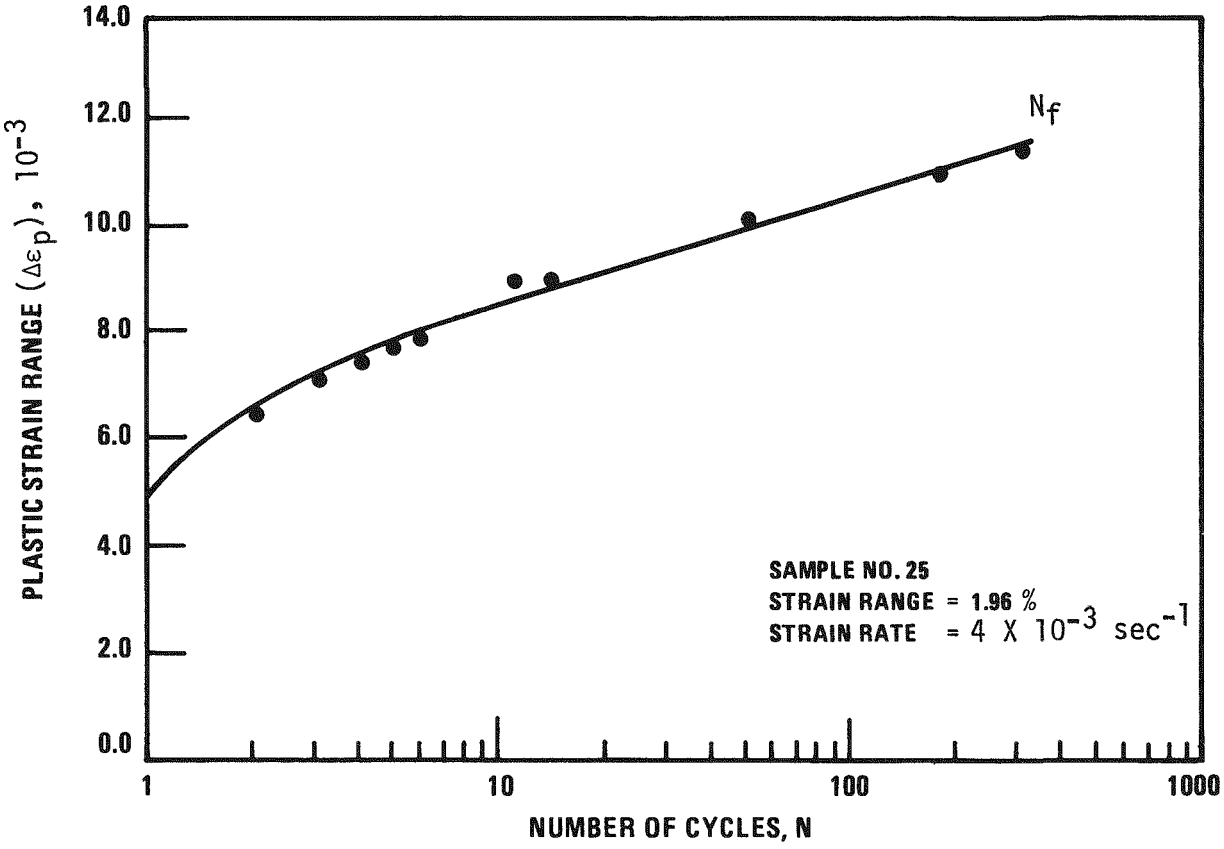

Figure 17. Cyclic Softening Of Inconel 718 (940°C S.A. + D.A.) At 538°C In Air

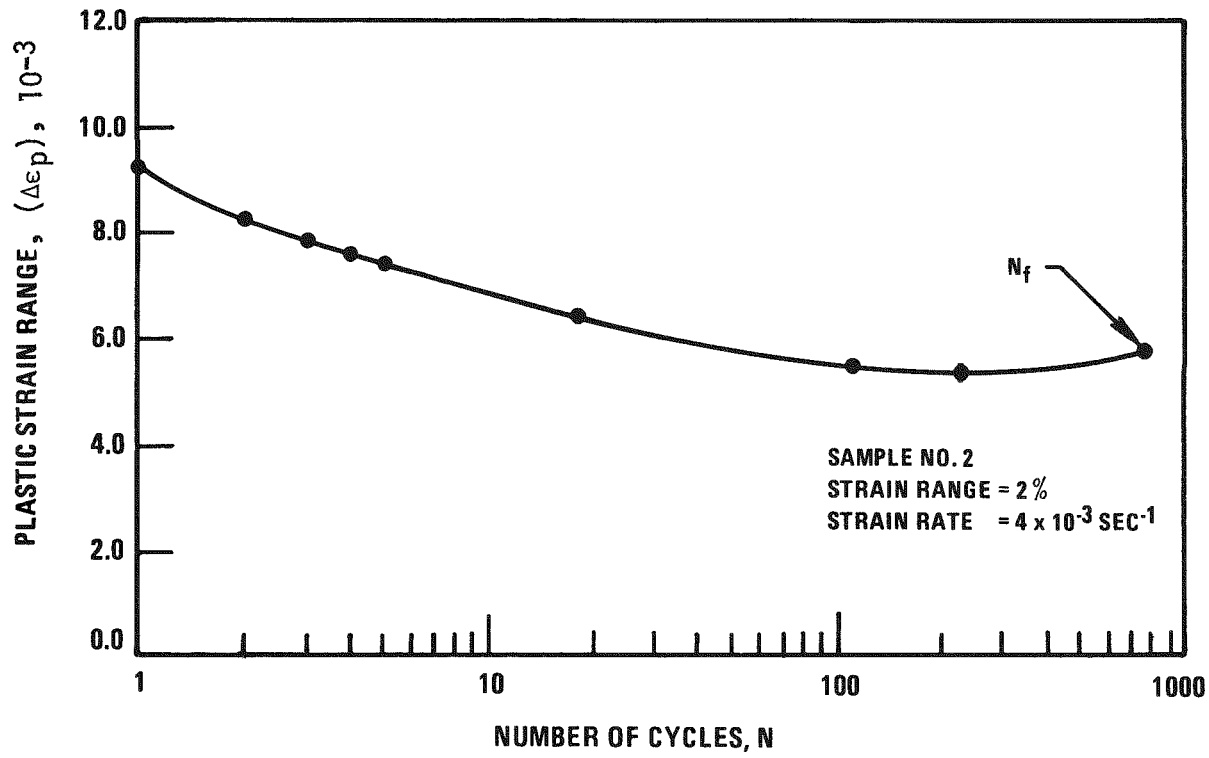

Figure 18. Cyclic Hardening Of INC-718 (1038°C S.A. + D.A.) At 538°C In Air

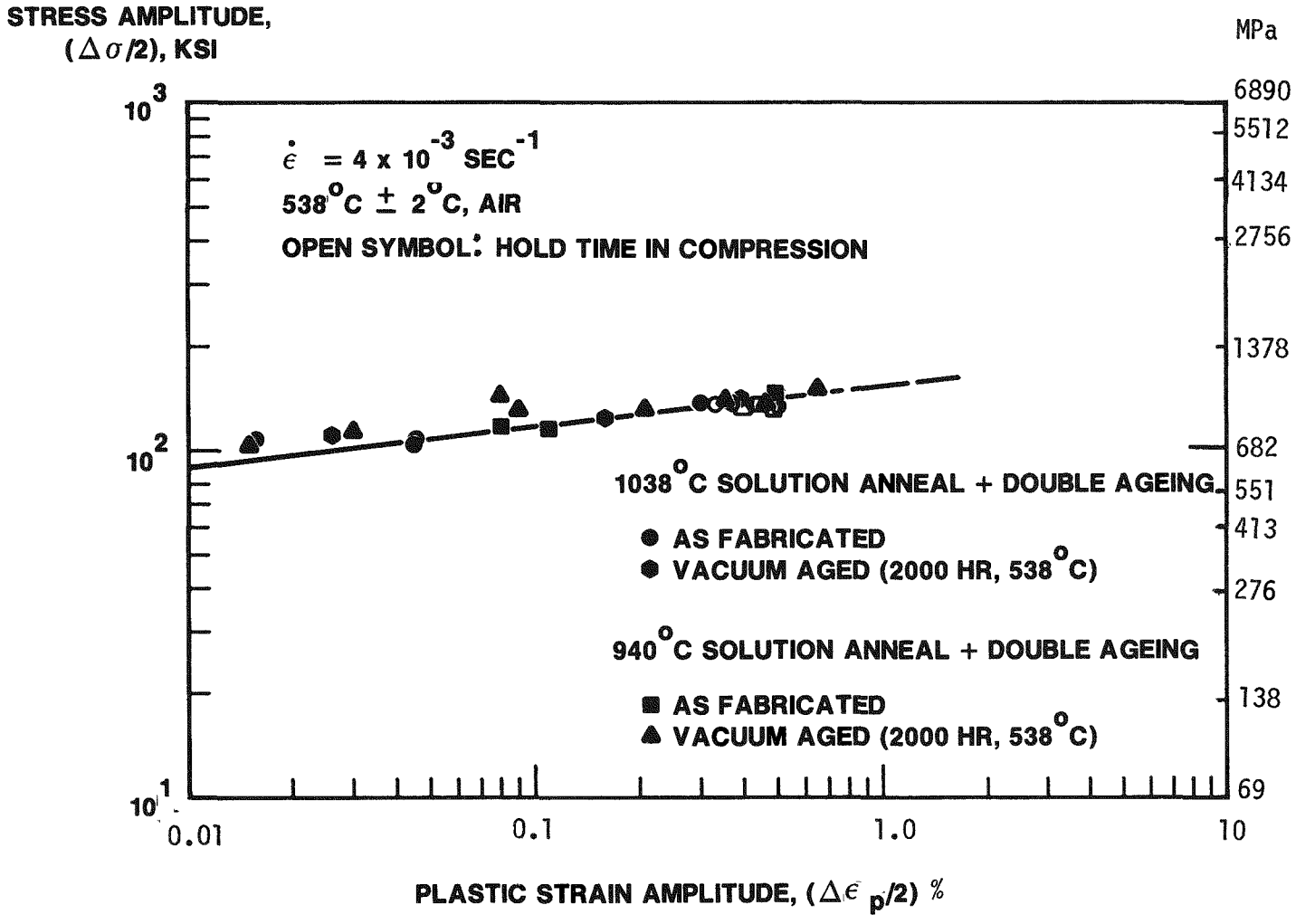

Figure 19. Stabilized Stress Amplitude Vs Plastic Strain Amplitude For INC-718 Low-Cycle Fatigue Testing

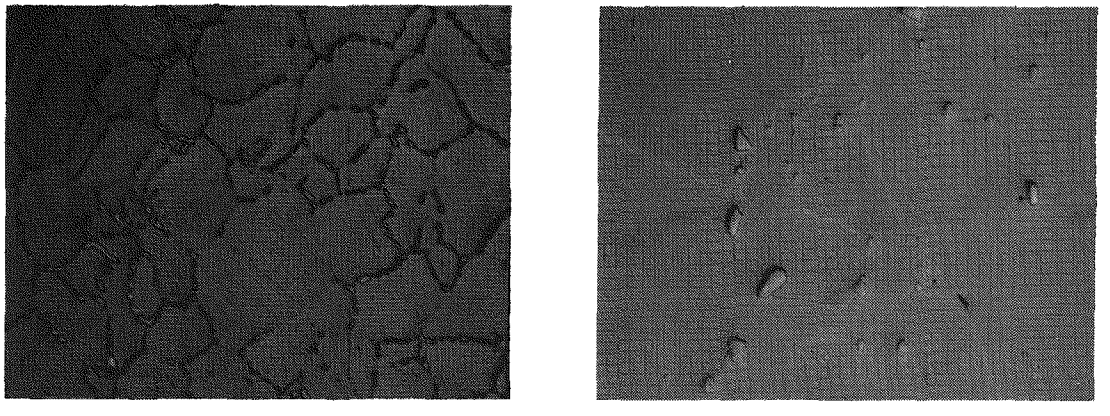

(a) (b)

(a) SOLUTION ANNEALED AT 940 °C PLUS DOUBLE AGEING (AMS 5596C), 1450X

(b) SOLUTION ANNEALED AT 1038 °C PLUS DOUBLE AGEING (AMS 5597A), 500X

Figure 20. Microstructure Of Inconel 718

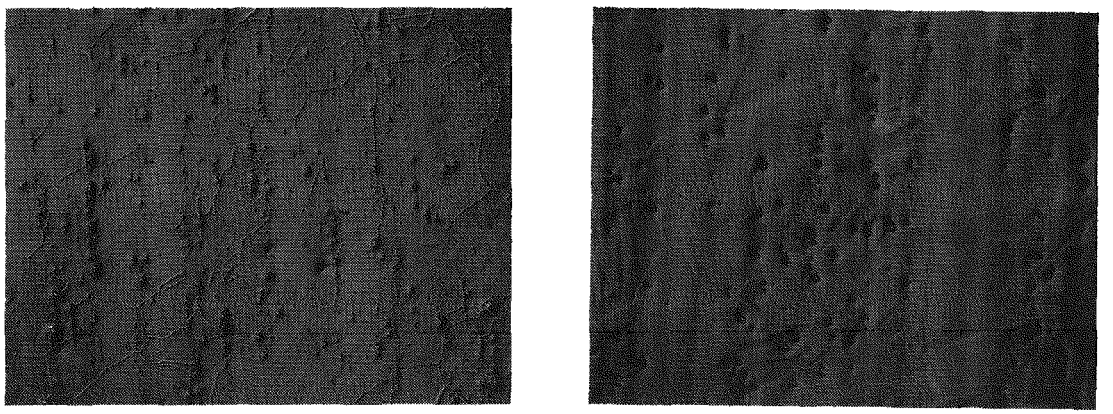

(a) (b)

(a) SOLUTION ANNEALED AT 1038°C PLUS DOUBLE AGEING (AMS 5597A) 100X

(b) 2000 HOURS VACUUM ANNEALING AT 538°C AFTER (a) TREATMENT ,100X

Figure 21. Microstructure Of As Received INC-718

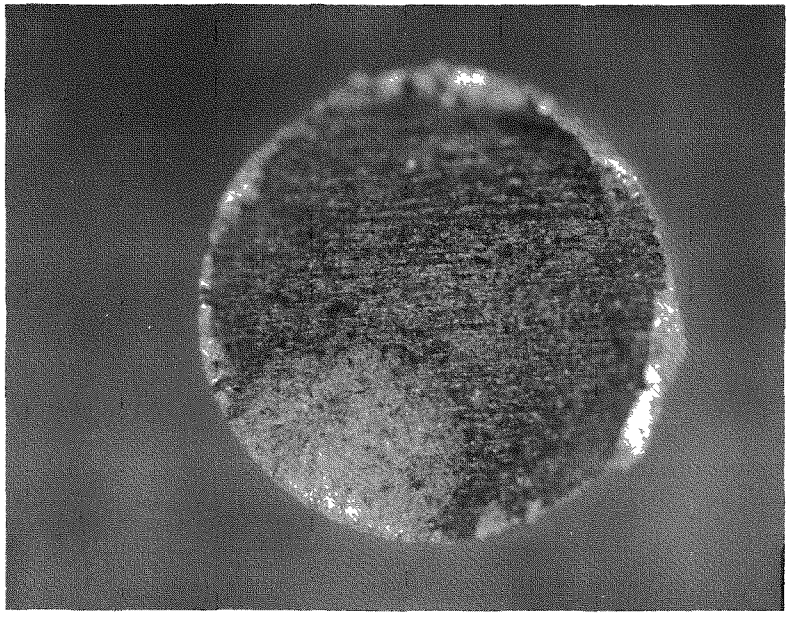

a

b

Figure 22 INC-718 940°C Solution Anneal + Duplex Age (AMS 5596C) Fatigue Tested at 538°C in Air, $\Delta\epsilon_t = .96 \times 10^{-2}$, $\dot{\epsilon} = 4 \times 10^{-3}$ sec^{-1}.

(a) Fractured Surface Showing the "Thumb" shaped Fatigue Crack, 7X

(b) Numerous Cracks Along the Gauge Length of the Fatigue Specimen, 7X

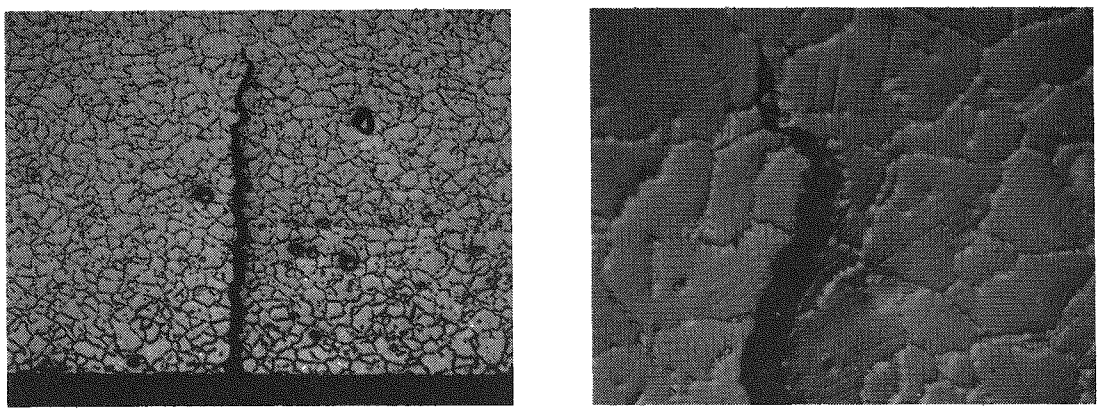

(a) (b)

(a) $\Delta\epsilon_t$ = 1.9%, $\dot{\epsilon}$ = 4 x 10^{-3} SEC^{-1}, 250X, 1% CHROMIC

(b) TIP OF THE CRACK SHOWN IN (a), 1450X

Figure 23. Fatigue Crack Of INC-718 (940°C S.A. + D.A.), 538°C In Air

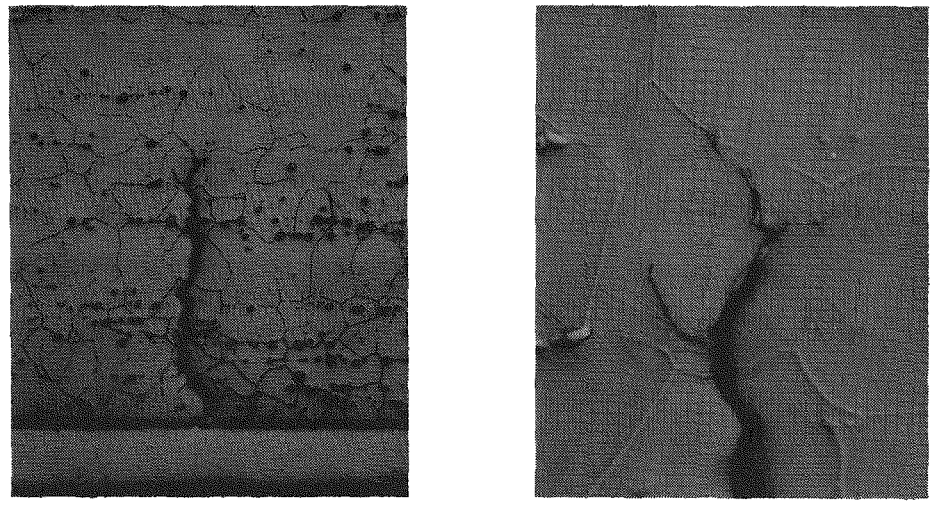

(a) (b)

(a) $\Delta\epsilon_t$ = 2%, $\dot{\epsilon}$ = 4 x 10^{-3} SEC^{-1}, 100X, 1% CHROMIC

(b) TIP OF THE CRACK SHOWN IN (a), 500X, GRAIN SIZE: ASTM 3-4

Figure 24. Fatigue Crack Of INC-718 (1038°C S.A. + D.A.), 538°C In Air

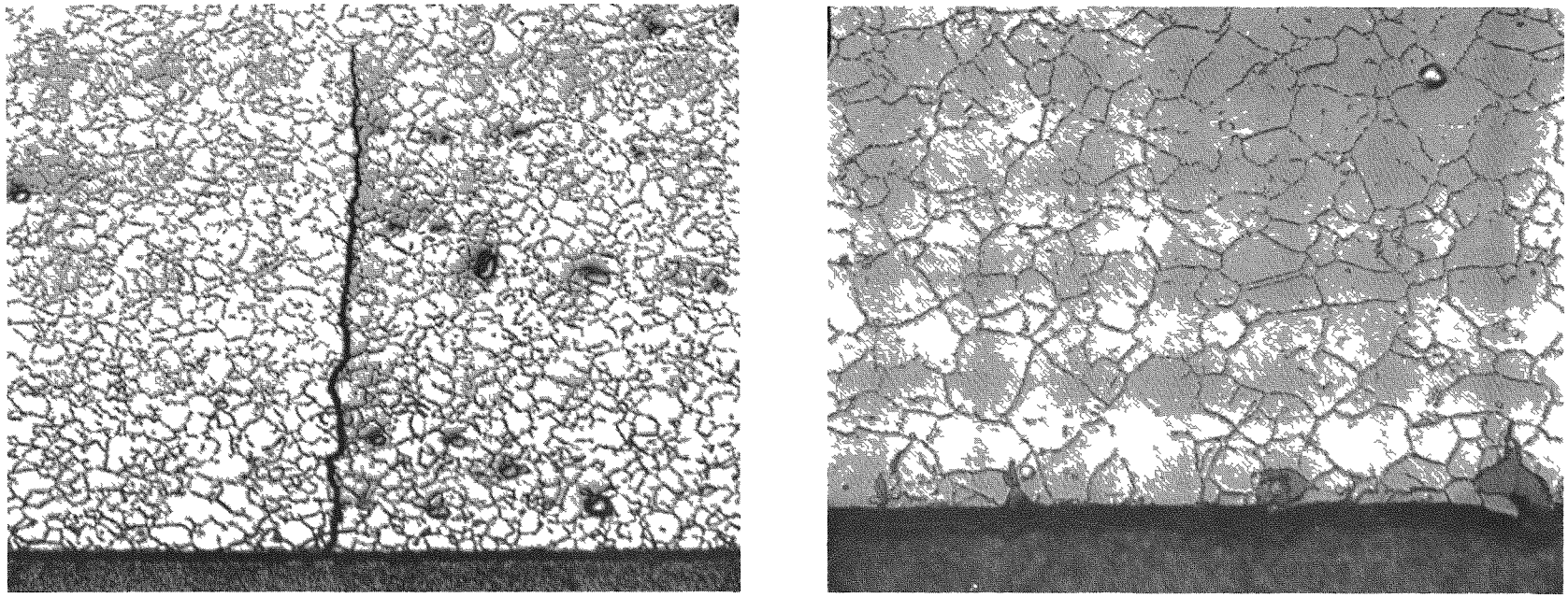

Figure 25 Fatigue Cracks in Inconel 718 Tested at 538°C in Air, $\dot{\varepsilon} = 4 \times 10^{-3}$ sec^{-1}.
(a) $\Delta\varepsilon_t$ = 2%, No Hold-Time. 250X
(b) $\Delta\varepsilon_t$ = 2%, With 60 min. Hold-Time in Compression. 500X

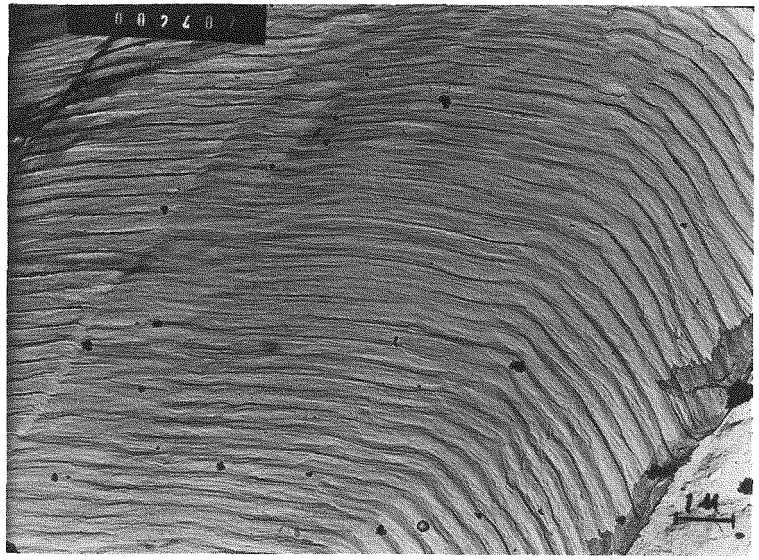

a

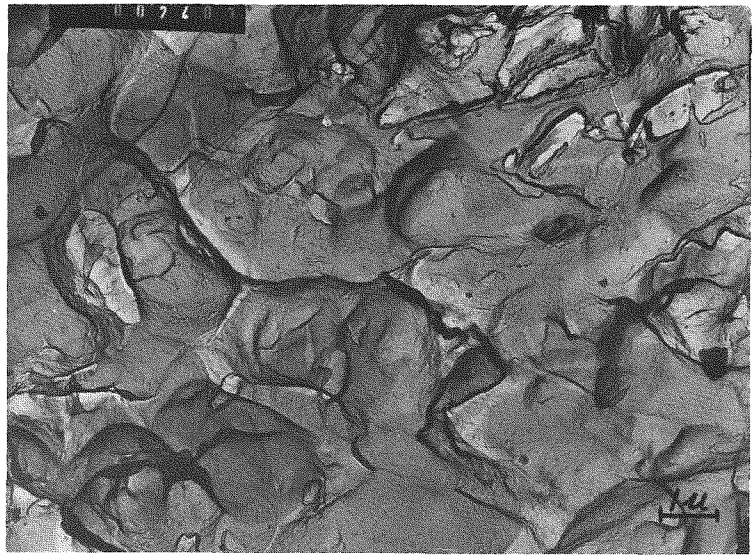

b

Figure 26 TEM Replica Micrographs showing (a) Striations (Brittle Failure) (b) Dimples (Ductile Failure) on the Fractured Surface of INC-718

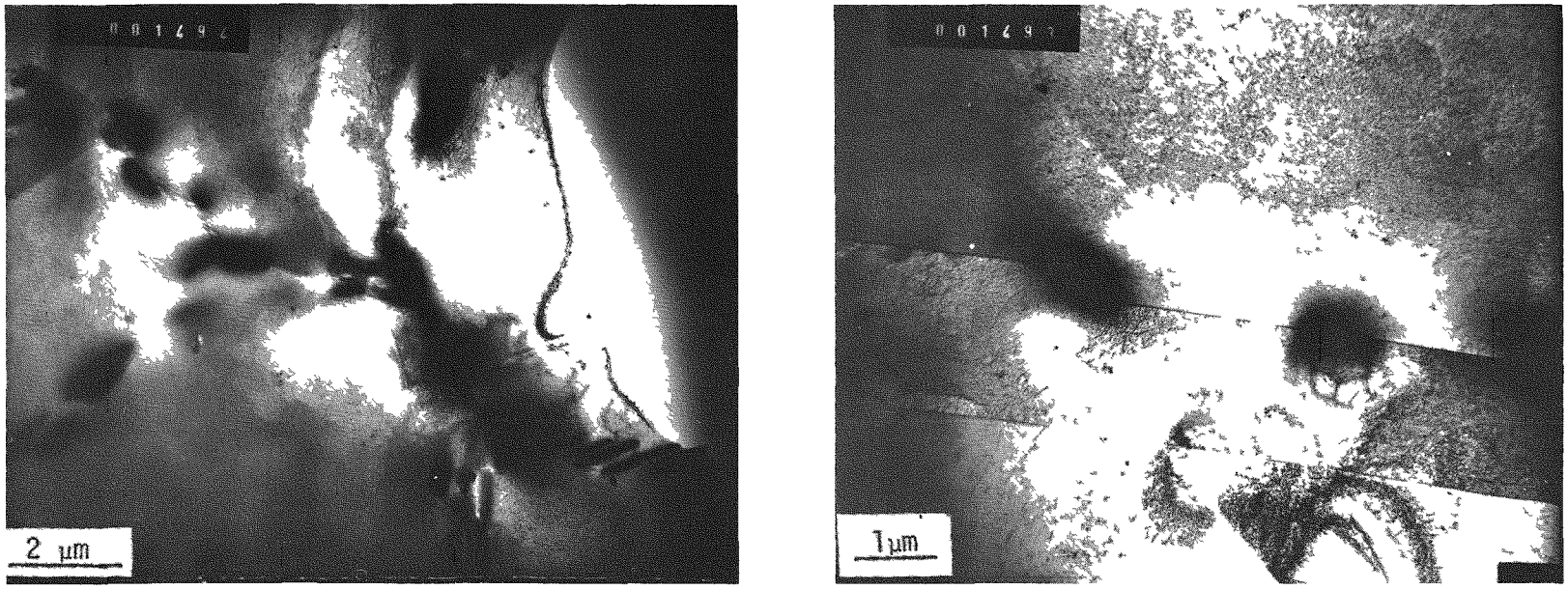

Figure 27 INC-718 940°C Solution Annealed + Duplex Aging (AMS 5596C) pre-test condition

(a) Carbide precipitation along grain boundaries

(b) Carbide precipitation along twin boundaries

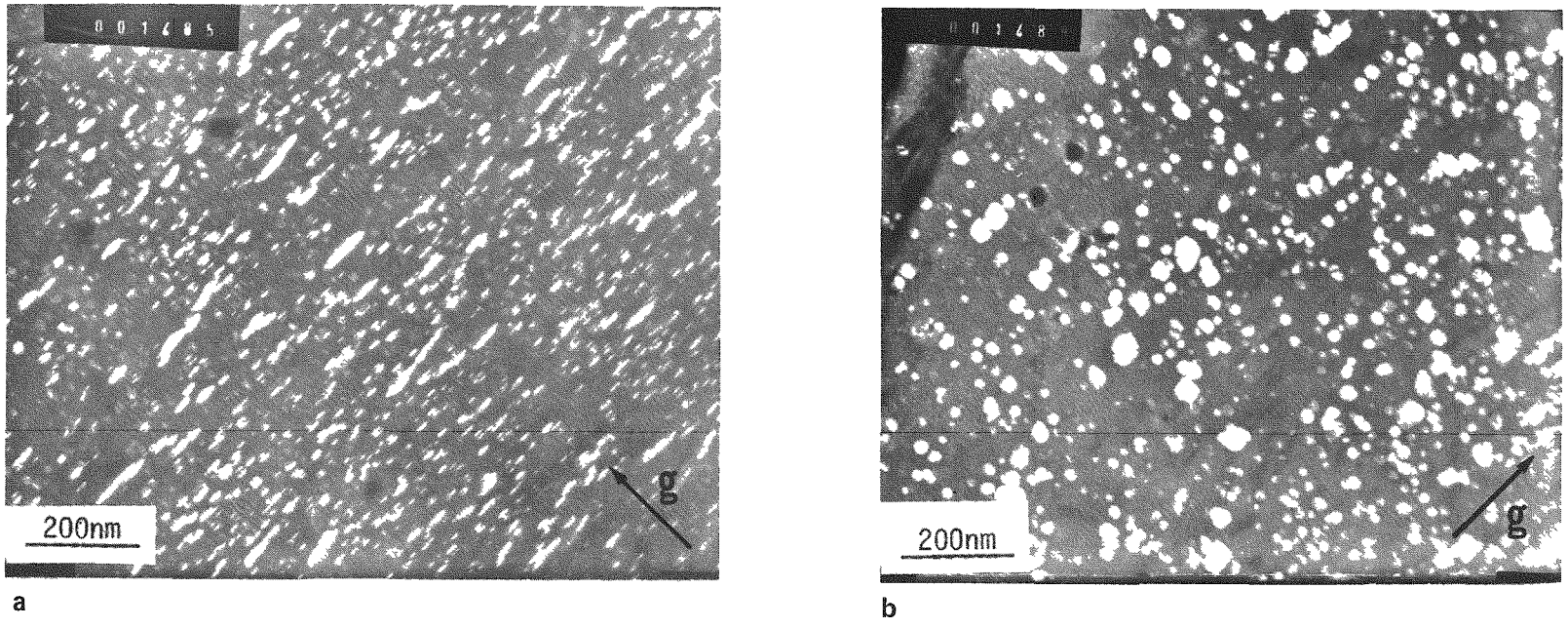

Figure 28 INC-718 940°C Solution Annealed + Duplex Aging (AMS 5596C) Pre-Test Condition

(a) Superlattice Dark-Field of ($\gamma' + \gamma''$), $\vec{g}$ = 001, $\vec{z} \cong [\bar{1}20]$

(b) Superlattice Dark-Field of γ'', g = 1 1/2 0, $\vec{z} = [\bar{1}20]$

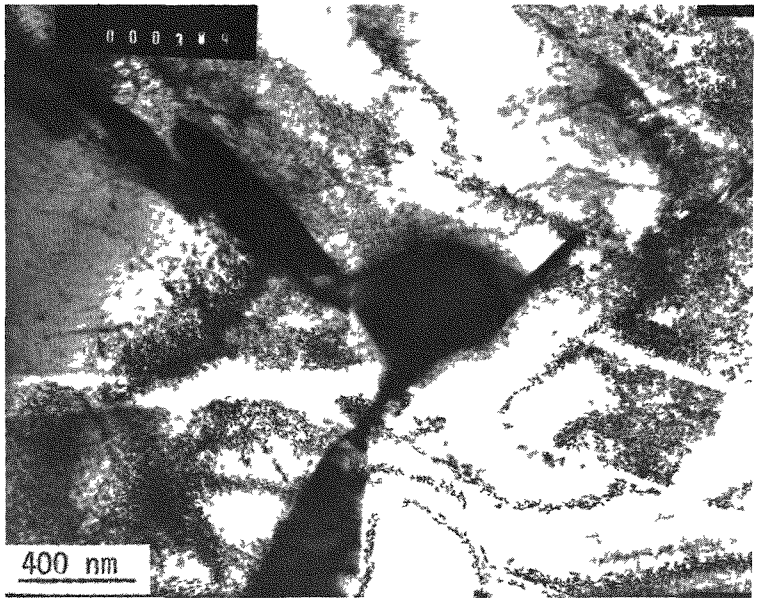

Figure 29 INC-718 940°C Solution Annealed + Duplex Aging (AMS 5596C) Post-Test Condition $\Delta\varepsilon_t$ = 2%, $\dot{\varepsilon}$ = 4 x 10^{-3} sec^{-1}, at 538°C in Air

Bright-Field Micrograph Showing Carbides Along Grain Boundaries and Slip Lines

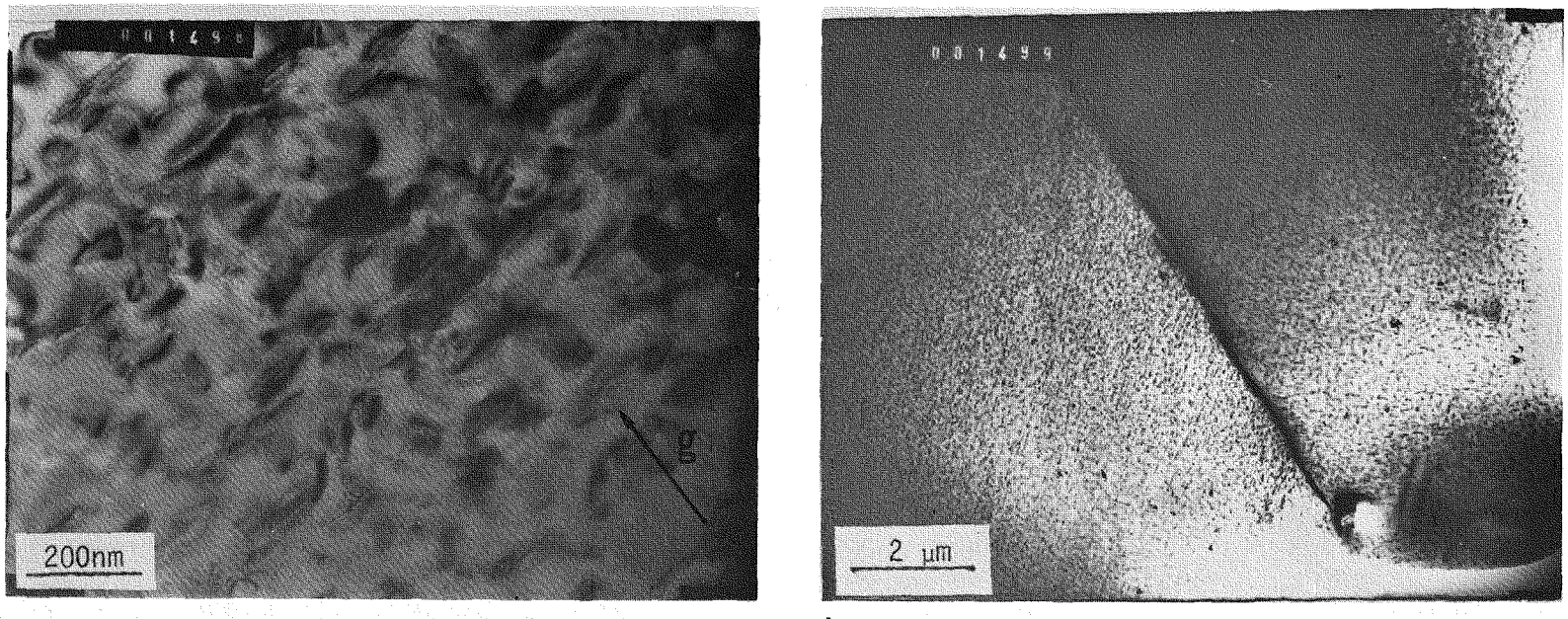

Figure 31 INC-718 1038°C Solution Annealed + Duplex Aging (AMS 5597A) Pre-test Condition

(a) Bright-Field TEM Micrograph of(γ'+ γ'') $\vec{g}$ = 002, $\vec{z} \cong$ [110]

(b) Carbides Precipitates Along Grain Boundaries

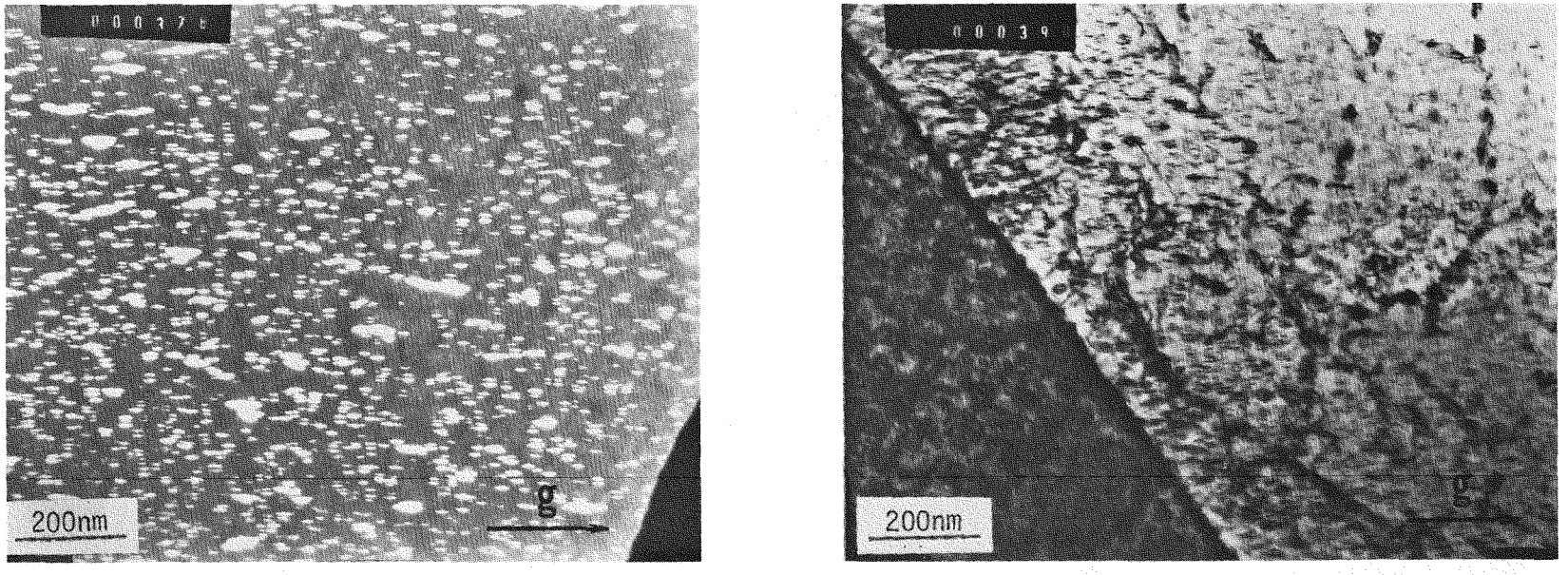

Figure 30 INC-718 940°C Solution Annealed + Duplex Aging (AMS 5596C) Post-Test Condition, $\Delta\varepsilon_t = 2\%$, $\dot{\varepsilon} = 4 \times 10^{-3}$ sec^{-1} at 538°C in Air.

(a) Superlattice Dark-Field of ($\gamma' + \gamma''$), $\vec{g} = 1\bar{1}0$, $\vec{z} \cong [110]$

(b) Bright-Field of ($\gamma' + \gamma''$), $\vec{g} = 1\bar{1}0$, $\vec{z} = [110]$

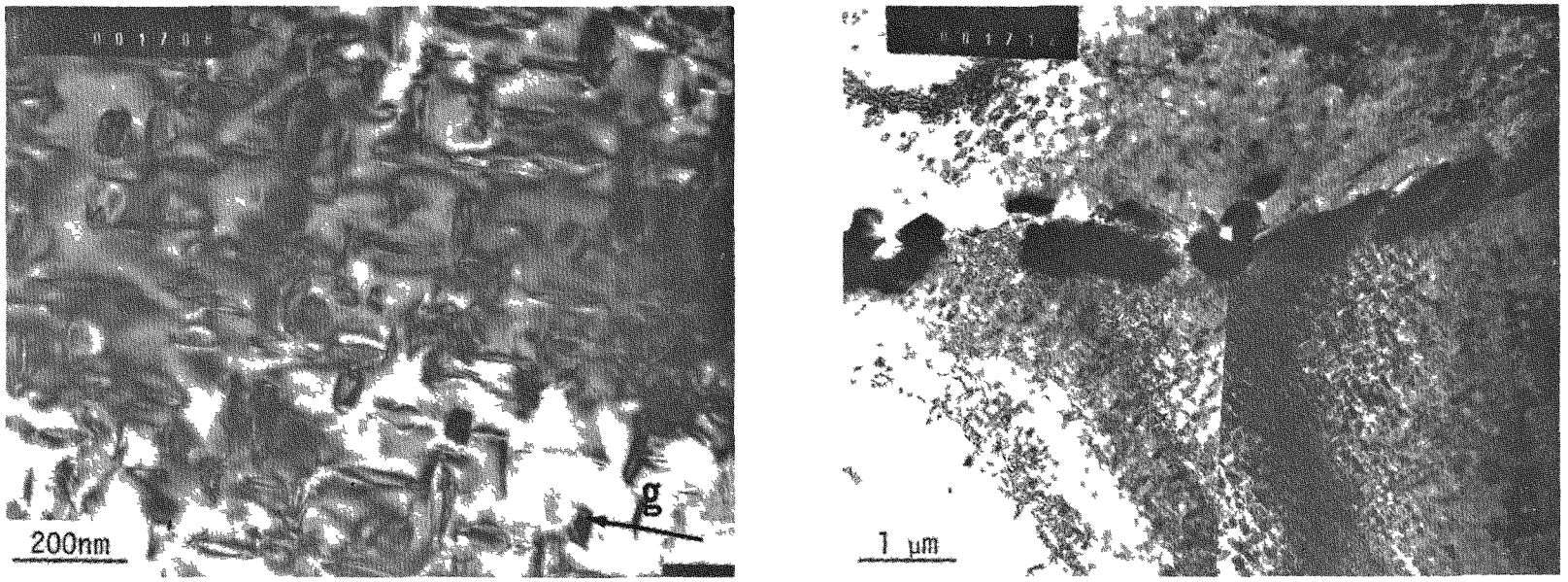

Figure 32 INC-718 1038°C Solution Annealed + Duplex Aging (AMS 5597A), $\Delta\varepsilon_t$ = 2%, $\dot{\varepsilon}$ = 4 x 10^{-3} sec^{-1}, 538°C in Air

(a) Bright-Field Micrograph of (γ'+ γ''), $\vec{g}$ = $1\bar{1}0$, $\vec{z} \cong$ [110]

(b) Bright-Field Micrograph Showing Carbides at Grain Boundaries and Dislocations

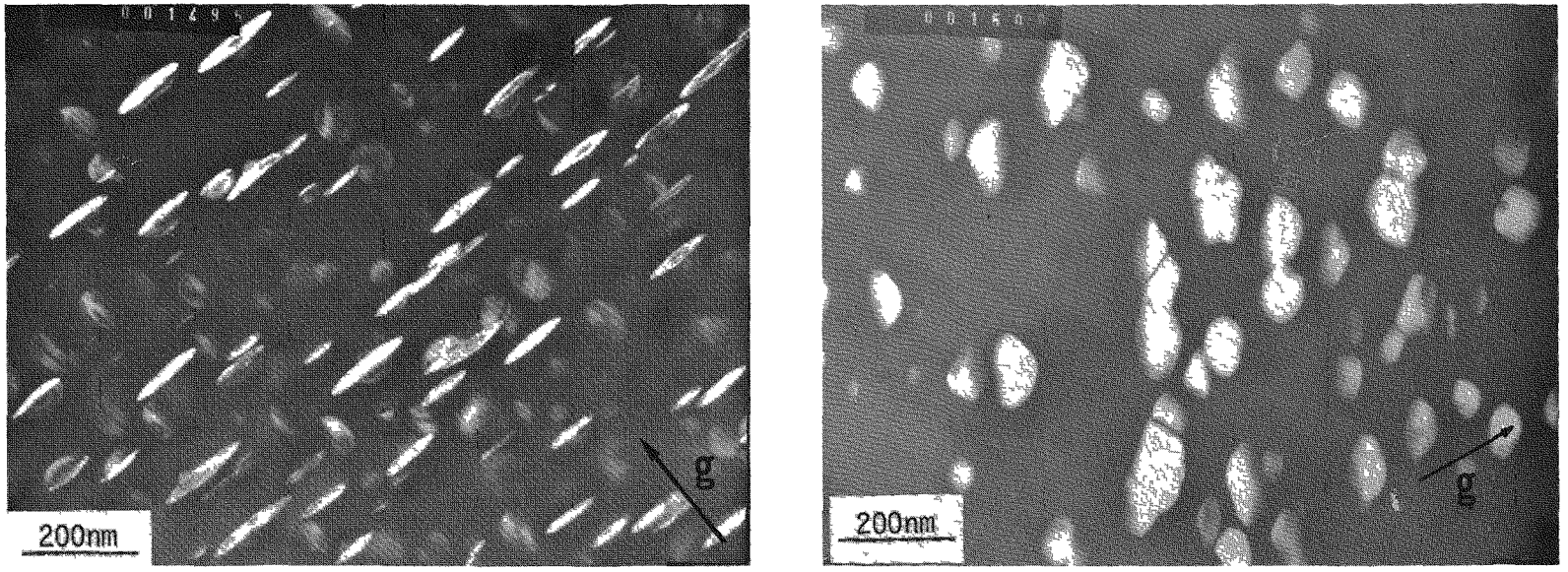

Figure 33 INC-718 1038°C Solution Annealed + Duplex Aging (AMS 5597A) Pre-Test Condition

(a) Superlattice Dark-Field of (γ'+ γ''), $\vec{g}$ = 001, $\vec{z}$ = [110]

(b) Superlattice Dark-Field of γ'', $\vec{g}$ = 01 1/2, $\vec{z} \cong [1\bar{1}2]$

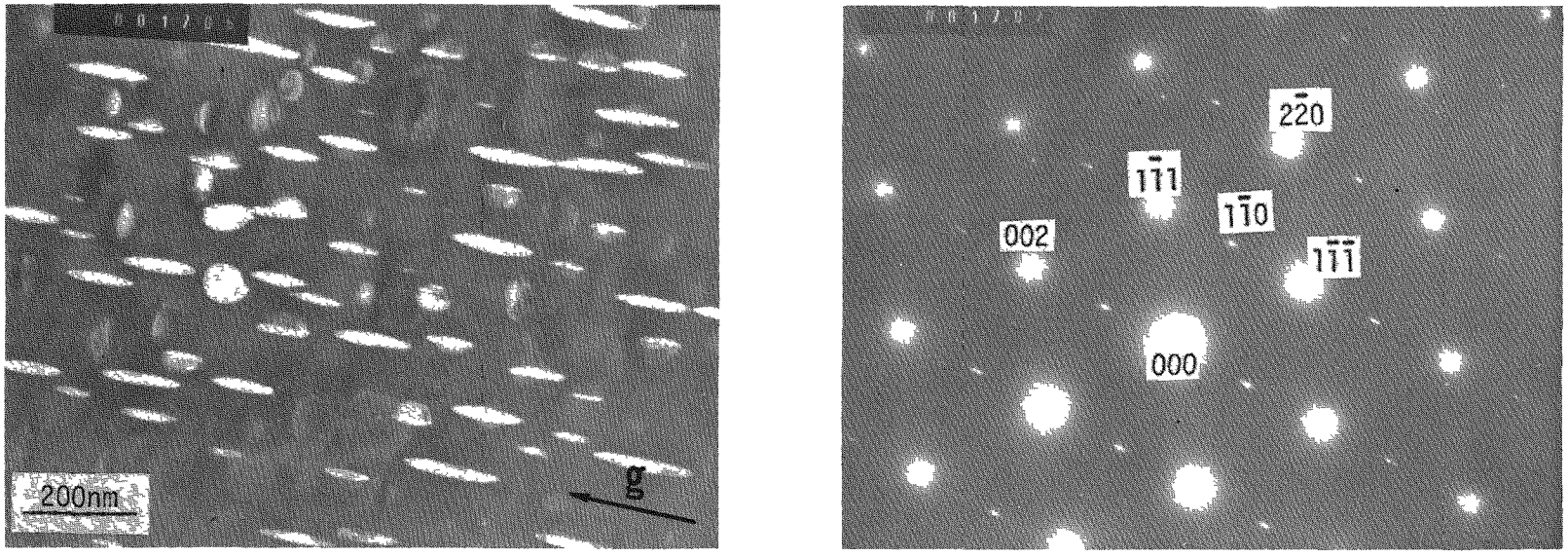

a b

Figure 34 INC-718 1038°C Solution Anneal + Duplex Aging (AMS 5597A), $\Delta\varepsilon_t$ = 2%, $\dot{\varepsilon}$ = 4 x $10^{-3}sec^{-1}$, 538°C in Air

(a) TEM Superlattice Dark-Field Micrograph of (γ' + γ''), $\vec{g} = 1\bar{1}0$, $\vec{z} \cong [110]$

(b) Corresponding SAD Pattern

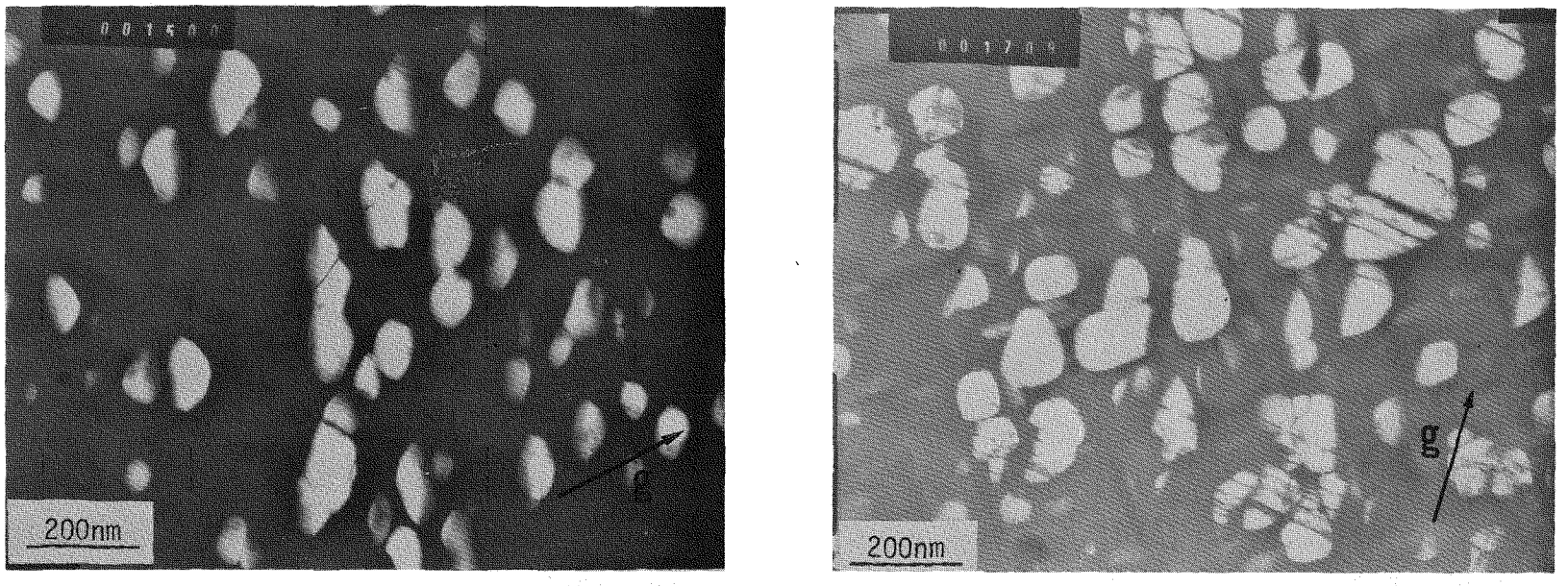

a b

Figure 35 INC-718 1038°C Solution Anneal + Duplex Aging (AMS 5597A)

(a) Superlattice Dark-Field of γ'', $\vec{g}$ = 01 1/2, $\vec{z}$ = $[1\bar{1}2]$, Pre-Test Condition

(b) Cutting of the γ'' During Fatigue Testing, $\vec{g}$ = $1\bar{1}0$, $\vec{z} \cong [111]$, $\Delta\varepsilon_t$ = 2%, $\dot{\varepsilon}$= 4 x $10^{-3}sec^{-1}$. 538°C in Air.

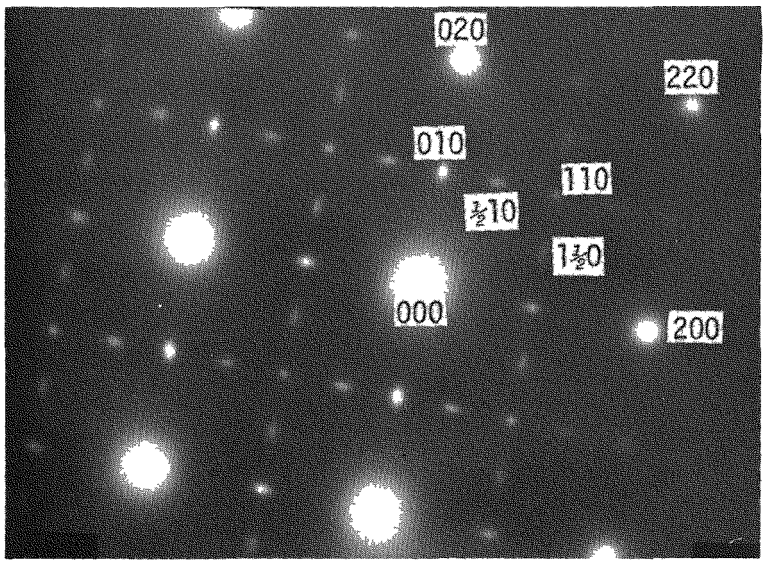

Figure 36 Electron diffraction pattern showing the existence of an ordered bct (DO_{22}) phase (γ''), $\vec{z}$ = [001] in Inconel 718 after heat treatments.

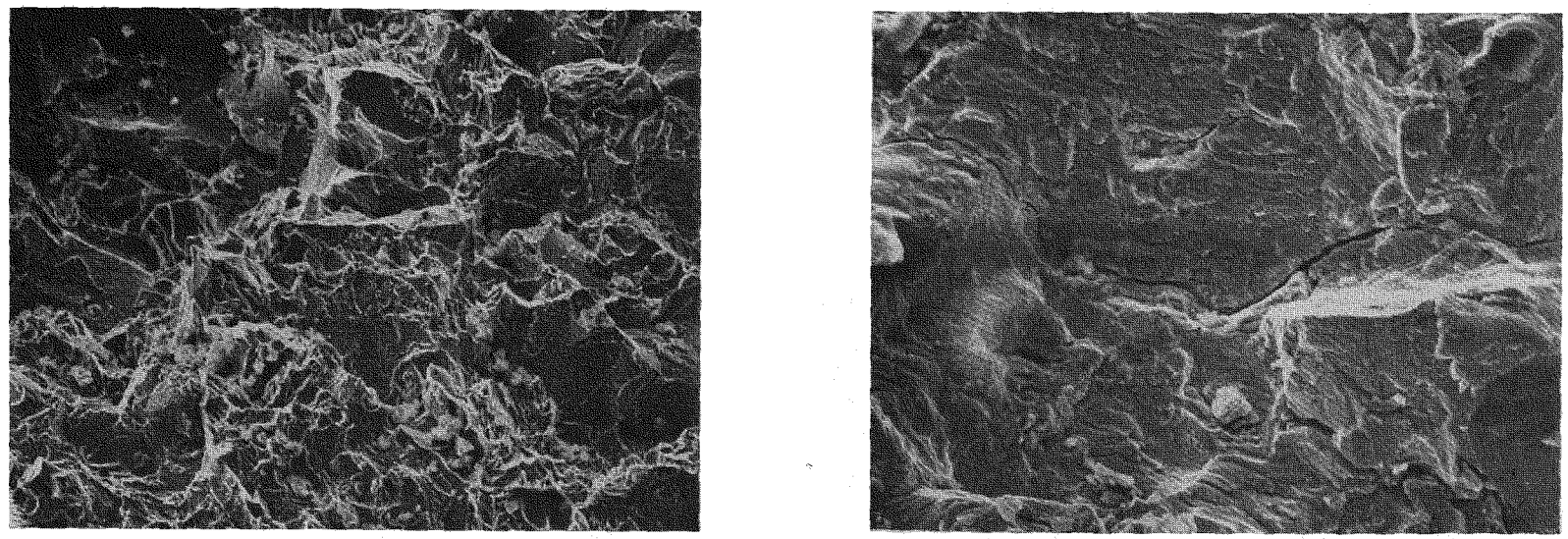

a b

Figure 37 SEM Fractography of Inconel 718 940°C Solution Annealed + Duplex Age (AMS 5596C), $\Delta\varepsilon_t$ = 2%, $\dot{\varepsilon}$ = 4 x $10^{-3}sec^{-1}$ at 538°C in Air.

(a) Transgranular Fracture and the Carbides, 45° tilt, 200X.

(b) Microcracks Approximately Parrallel to the Loading Direction, 45° tilt, 500X.

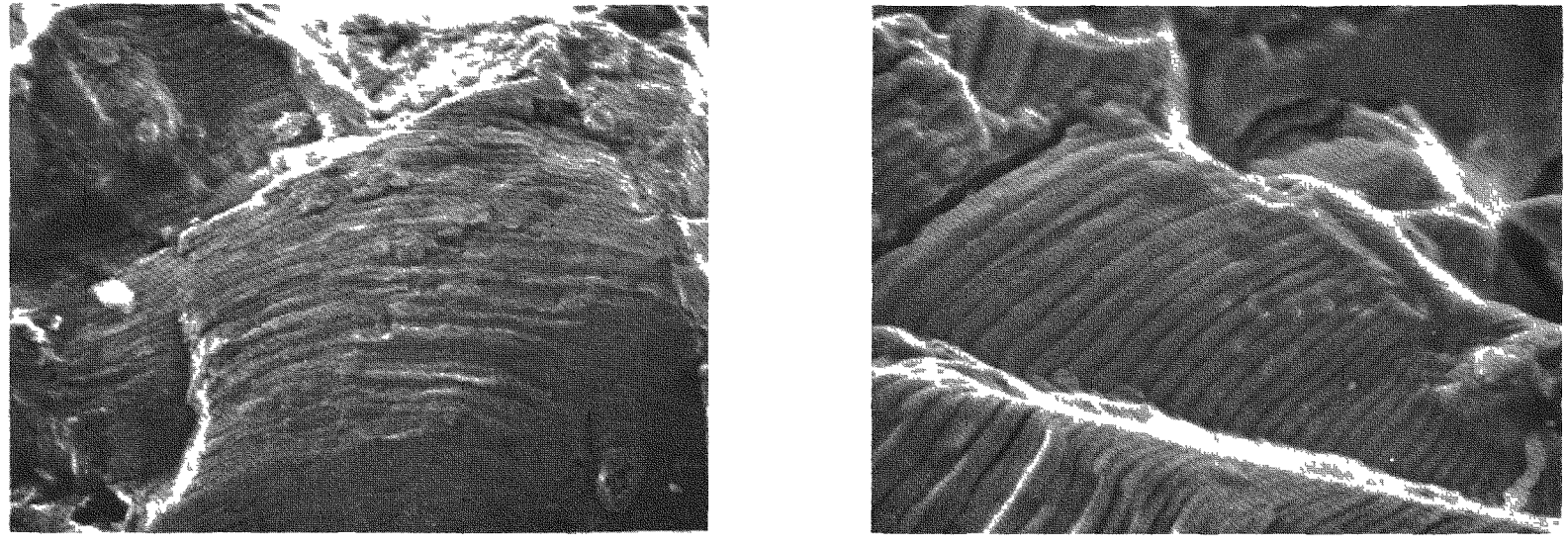

a b

Figure 38 SEM Fractography of INC-718 940°C Solution Annealed + Duplex Age (AMS 5596C), $\Delta\varepsilon_t$ = 2%, $\dot{\varepsilon}$ = 4 X 10^{-3} sec^{-1}, at 538°C in Air.

(a) Fatigue Striations, 1000X, 45° tilt.

(b) Close View of the Striations and the Microcracks, 2000X, 45° tilt.

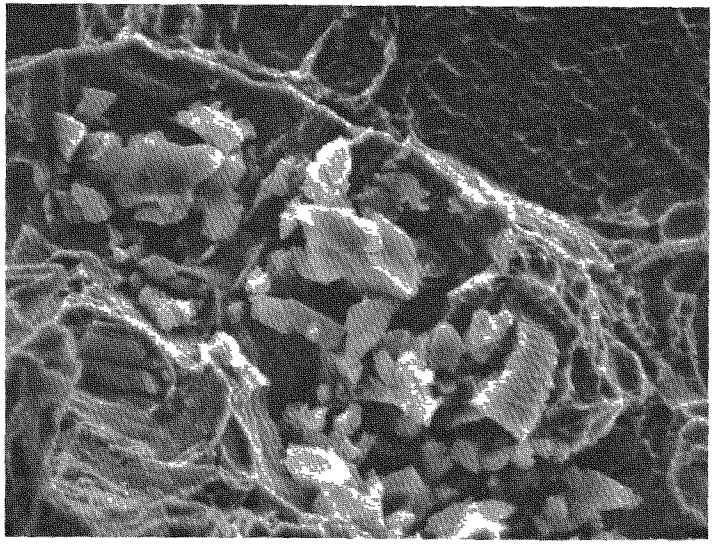

a

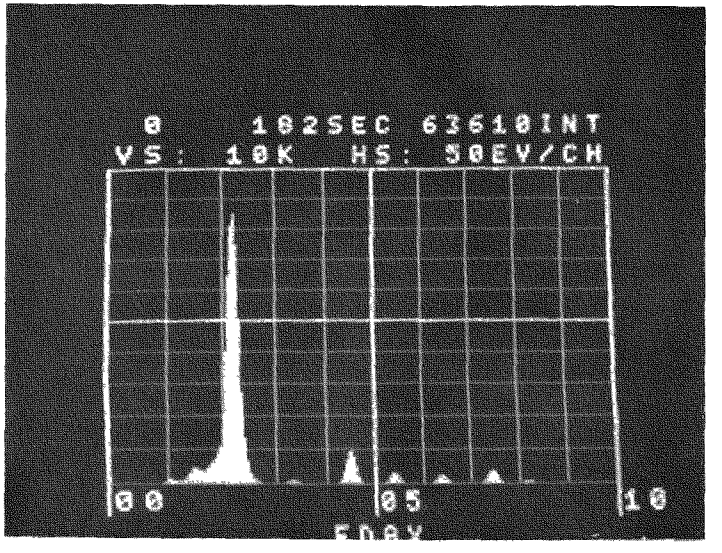

b

Figure 39 INC-718 1038°C Solution Anneal + Duplex Age (AMS 5597A), $\Delta\varepsilon_t$ = 2 %
$\dot{\varepsilon}$ = 4 x $10^{-3}sec^{-1}$ at 538°C in Air.

(a) SEM Fractograph Showing the Presence of the Carbide Particles, 1600X.

(b) Corresponding EDAX Scan of the Carbide Phase

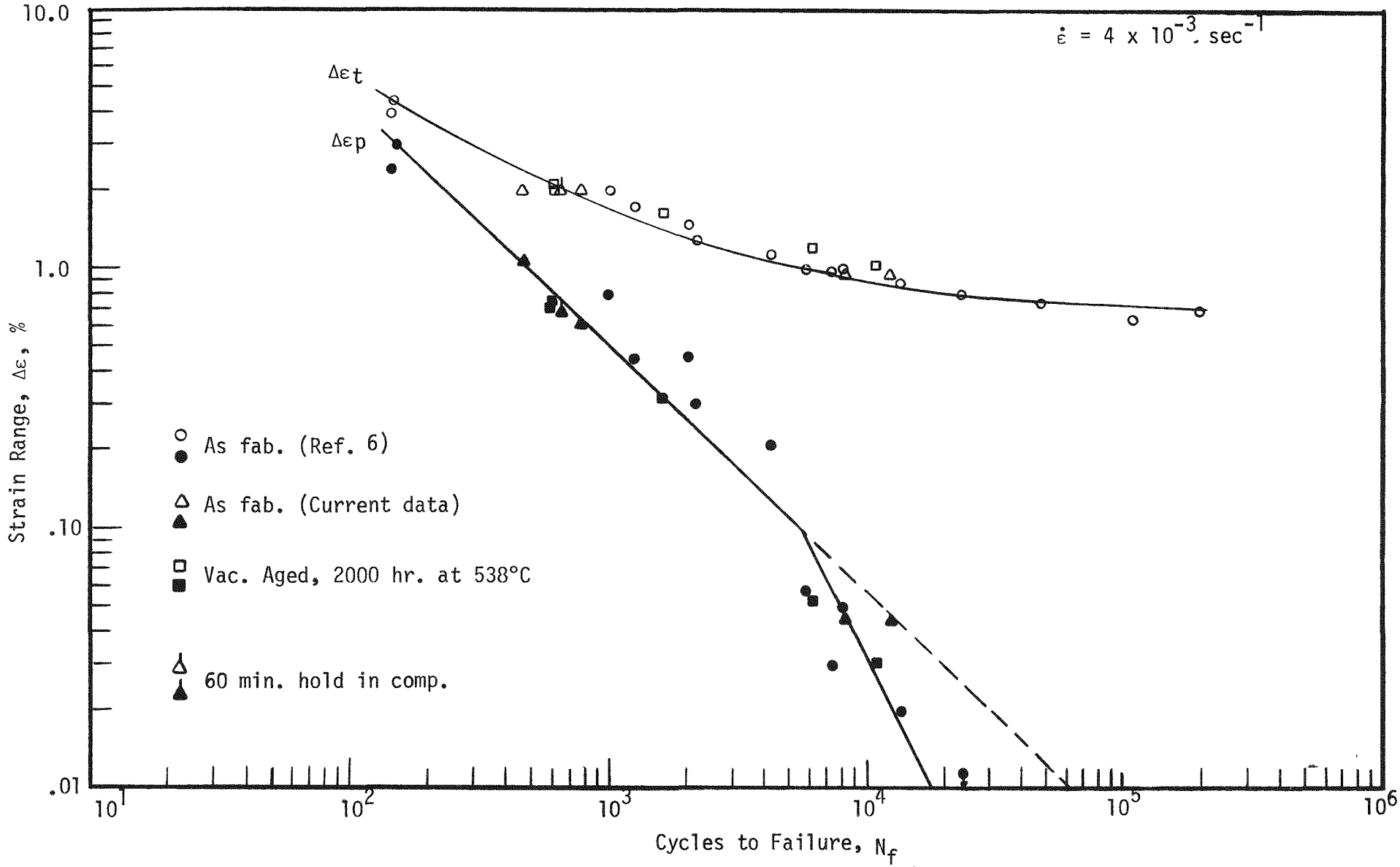

Figure 40 Low-Cycle Fatigue Life of Inconel 718 (1038°C S. A. + D. A.) at 538°C in Air

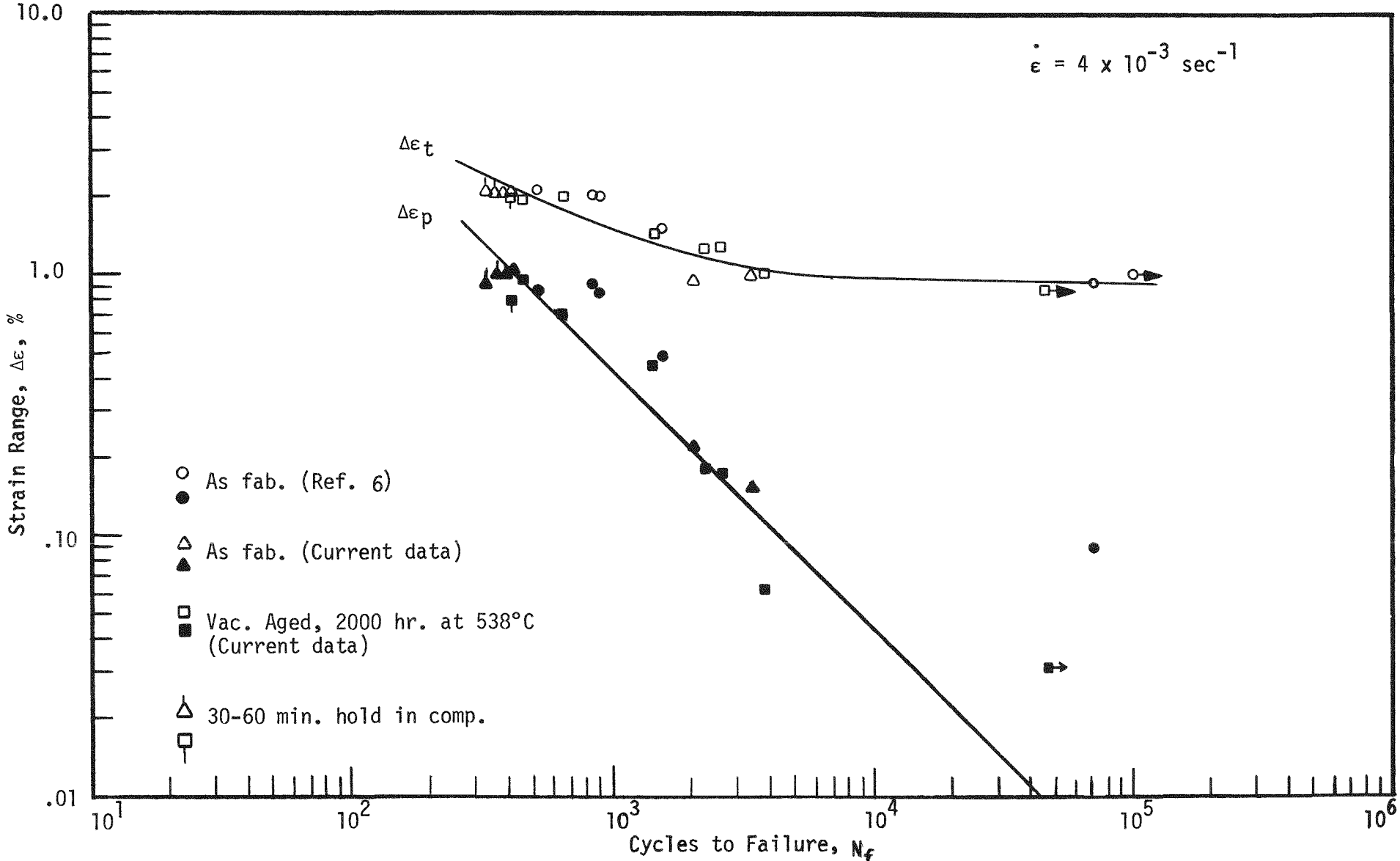

Figure 41 Low-Cycle Fatigue Life of Inconel (940°C S. A. + D. A.) at 538°C in Air

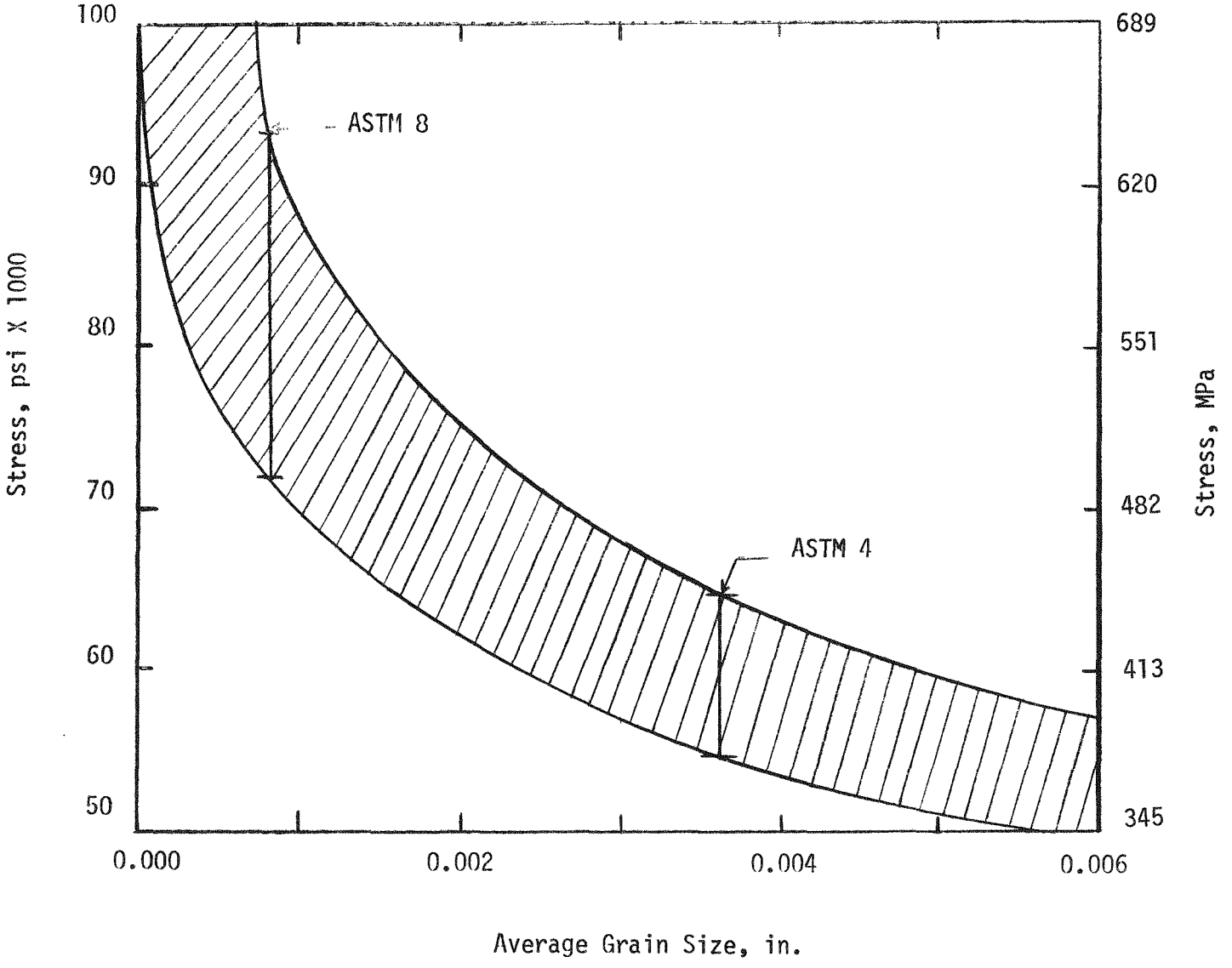

Figure 42 Effect of grain size on endurance limit (10^8 cycles) of Inconel 718 plate annealed and aged in accordance with AMS 5596B. (Ref. 7)